


## Bohr Hamiltonian with sextic potential for $\gamma$ -rigid prolate nuclei with deformation-dependent mass term

M. Oulne<sup>\*</sup> and I. Tagdamte<sup>†</sup>

*High Energy Physics and Astrophysics Laboratory, Department of Physics, Faculty of Sciences Semailia, Cadi Ayyad University, P.O. Box 2390, Marrakesh 40000, Morocco*

 (Received 18 August 2022; accepted 10 November 2022; published 12 December 2022)

The main aim of the present paper is to solve the eigenvalues problem with the Bohr collective Hamiltonian for  $\gamma$ -rigid nuclei within a model we have elaborated by combining two model approaches: the quantum mechanical formalism, namely, deformation-dependent mass formalism (DDM), and the anharmonic sextic oscillator potential for the variable  $\beta$  and  $\gamma = 0$ . The model developed in this way is conventionally called the sextic and DDM approach. Analytical expressions for energy spectra are conjointly derived by means of quasixact solvability and a quantum perturbation method. Due to the scaling property of the problem, the energy and  $B(E2)$  transition ratios depend on two free parameters apart from an integer number which limits the number of allowed states. Numerical results are given for 35 nuclei— $^{98-108}\text{Ru}$ ,  $^{100-102}\text{Mo}$ ,  $^{116-130}\text{Xe}$ ,  $^{180-196}\text{Pt}$ ,  $^{172}\text{Os}$ ,  $^{146-150}\text{Nd}$ ,  $^{132-134}\text{Ce}$ ,  $^{154}\text{Gd}$ ,  $^{156}\text{Dy}$ , and  $^{150-152}\text{Sm}$ —revealing a good agreement with experiment. Moreover, as proved for the first time by Bonatsos *et al.* [D. Bonatsos, P. Georgoudis, D. Lenis, N. Minkov, and C. Quesne, *Phys. Lett. B* **683**, 264 (2010)], the dependence of the mass on the deformation with the sextic potential moderates the increase of the moment of inertia with the deformation, removing an important drawback that has been revealed in the constant mass case [Buganu and Budaca, *J. Phys. G: Nucl. Part. Phys.* **42**, 105106 (2015)]. Additionally, the correlation between the DDM and the minimal length formalism persists for the sextic potential. Finally, the DDM effects on the shape phase transition for the most numerous isotopic chains, namely, Ru, Xe, Nd, and Pt, have been duly investigated.

DOI: [10.1103/PhysRevC.106.064313](https://doi.org/10.1103/PhysRevC.106.064313)

### I. INTRODUCTION

Most nuclear models are focused on explaining the atomic nuclei structure. One of the well-known examples is the Bohr-Mottelson model [1,2]. This model is based on the coupling between rotational and vibrational motions of the shape defined by intrinsic deformation variables  $\beta$  and  $\gamma$ , namely, deviation from sphericity and deviation from axiality, respectively. Also, it reflects some theoretical aspects in the physical observables wherein a good agreement with experimental data has been observed [3]. However, various model potentials have been used in the Bohr Hamiltonian for the purpose of describing suitable shape phase transitions in atomic nuclei, particularly, those which are related to the topic of critical point symmetries (CPSs), particularly,  $E(5)$  [4],  $X(5)$  [5],  $Y(5)$  [6], and  $Z(5)$  [7], which describe the nuclei situated in the critical points of the shape phase transitions from spherical vibrator [ $U(5)$ ] to  $\gamma$ -unstable [ $O(6)$ ] nuclei, from spherical vibrator to prolate rotor [ $SU(3)$ ], from axial rotor to triaxial rotor, and from prolate rotor to oblate rotor, respectively.

On the other hand, in recent years there has been an increased interest in the study of quantum mechanical systems with a position-dependent effective mass, especially in nuclear physics where several theoretical comparisons with experimental data have shown that the mass tensor of the col-

lective Bohr Hamiltonian cannot be considered as a constant and should be taken as a function of the collective coordinates. It should be noted that the deformation-dependent mass formalism (DDM) is not particularly new and has been used for many years. Initially proposed to describe impurities in crystals [8–10], it has also become an essential ingredient in the description of electronic properties of semiconductors [11] and quantum dots [12]. It was introduced for the first time in nuclear physics by Bonatsos *et al.* [13,14]; also, it has been used in several works [15–18].

Moreover, various model potentials have been used to construct analytical solutions of the Schrödinger equation associated with the Bohr Hamiltonian with DDM formalism, but there is no previous research using the sextic potential with the quantum concept of DDM. So, the overall goal of this paper is to propose solutions for the Bohr Hamiltonian in the frame of a DDM in  $\gamma$ -rigid mode  $X(3)$  with anharmonic sextic oscillator potential for the variable  $\beta$  and with  $\gamma$  frozen to  $\gamma = 0$ , to obtain the expressions of eigenvalues and wave functions by means conjointly of quasixact solvability (QES) [19] and a quantum perturbation method (QPM) [20] and to study the DDM effect on the energy spectra, the transition rates, and the variation of moment of inertia in axial symmetry shape.

In general, the sextic potential is given by [21,22]

$$V(a, b, c; \beta) = \frac{\hbar^2}{2B}((b^2 - 4ac)\beta^2 + 2ab\beta^4 + a^2\beta^6), \quad a \neq 0, \quad (1)$$

\*oulne@uca.ac.ma

†Corresponding author: tagdamte.imad@gmail.com

where  $a$ ,  $b$ , and  $c$  are three parameters. Note that for  $a = 0$ , the sextic potential becomes the harmonic oscillator potential.

An important remark is that the sextic potential, which is a quasireactly solvable phenomenological potential, is one of the best candidate potentials for the description of the spherical to deformed shape phase transition. This is revealed from the fact that it can have a spherical minimum, a deformed one, concurrently spherical and deformed minima, or a flat shape. Such a potential was used for the first time in the Bohr framework by Levai and Arias [23,24], and later on in several works related to the nuclear structure [21,22,25–29]. The present model is called the sextic and DDM approach [X(3)-SDDMA] and the plan of the paper is as follows: the second section will focus on the theoretical framework of the model and will be divided in five subsections: In the first one we briefly recall the theoretical background of DDM formalism, in the second one we will apply the DDM formalism on the  $\gamma$ -rigid Bohr Hamiltonian with the sextic potential, solutions of the Schrödinger equation in the case of constant mass parameter are given in the third subsection by means of QES, while the correction to the energy spectrum of the system is given in the fourth subsection by QPM. In Sec. III the numerical applications are presented and the results are discussed from both theoretical and experimental points of view. Finally, Sec. IV contains our conclusions.

## II. THEORETICAL FRAMEWORK

In the present section, we will give briefly the background of the DDM, consider the case where the Schrödinger equation contains a position-dependent mass, and then derive the analytical expressions for energy spectra by means conjointly of QES and a QPM.

### A. DDM formalism

When tensor mass depends on deformation coordinates, it does not commute with momentum  $p = -i\hbar\nabla$ . In order to overcome such a problem, Von Roos proposed a general hermitian Hamiltonian including some new parameters given by [30]

$$H_{\text{DDM}} = -\frac{\hbar^2}{4} [B^{\delta'}(\beta)\nabla B^{\kappa'}(\beta)\nabla B^{\lambda'}(\beta) + B^{\lambda'}(\beta)\nabla B^{\kappa'}(\beta)\nabla B^{\delta'}(\beta)] + V(\beta), \quad (2)$$

where  $V(\beta)$  is some potential and the parameters  $\delta'$ ,  $\kappa'$ , and  $\lambda'$  are constrained by the condition  $\delta' + \kappa' + \lambda' = -1$ . By expressing the position-dependent mass  $B(\beta)$  as

$$B(\beta) = B_0 M(\beta) \quad M(\beta) = \frac{1}{f^2(\beta)}, \quad (3)$$

where  $B_0$  is a constant mass and  $M(\beta)$  is a dimensionless position-dependent mass, Eq. (2) can be rewritten as

$$H_{\text{DDM}} = -\frac{\hbar^2}{4B_0} [f^\delta(\beta)\nabla f^\kappa(\beta)\nabla f^\lambda(\beta) + f^\lambda(\beta)\nabla f^\kappa(\beta)\nabla f^\delta(\beta)] + V(\beta), \quad (4)$$

where  $\delta + \kappa + \lambda = 2$  and the expression  $f^\delta\nabla f^\kappa\nabla f^\lambda$  is developed as follows:

$$\begin{aligned} f^\delta\nabla f^\kappa\nabla f^\lambda &= f^\delta\nabla f^{\frac{1}{2}-\delta} f f^{\frac{1}{2}-\lambda}\nabla f^\lambda \\ &= \left[ f^{1/2}\nabla + \left(\frac{1}{2} - \delta\right) f^{-1/2}\nabla f \right] f \\ &\quad \times \left[ \nabla f^{1/2} - \left(\frac{1}{2} - \lambda\right) f^{-1/2}\nabla f \right] \\ &= \sqrt{f}\nabla f\nabla\sqrt{f} + (\lambda - \delta)\sqrt{f}\nabla f \cdot \nabla\sqrt{f} \\ &\quad - \left(\frac{1}{2} - \lambda\right) f\nabla^2 f - \left(\frac{1}{2} - \delta\right)\left(\frac{1}{2} - \lambda\right) \\ &\quad \times (\nabla f)^2, \end{aligned} \quad (5)$$

and we indeed obtain

$$\begin{aligned} f^\delta\nabla f^\kappa\nabla f^\lambda + f^\lambda\nabla f^\kappa\nabla f^\delta \\ = 2\sqrt{f}\nabla f\nabla\sqrt{f} - (1 - \delta - \lambda)f\nabla^2 f \\ - 2\left(\frac{1}{2} - \delta\right)\left(\frac{1}{2} - \lambda\right)(\nabla f)^2. \end{aligned} \quad (6)$$

Finally the Hamiltonian (4) becomes

$$H_{\text{DDM}} = -\frac{\hbar^2}{2B_0}\sqrt{f(\beta)}\nabla f(\beta)\nabla\sqrt{f(\beta)} + V_{\text{eff}}(\beta), \quad (7)$$

where  $V_{\text{eff}}(\beta)$  is the effective potential given by

$$V_{\text{eff}}(\beta) = V(\beta) + \frac{\hbar^2}{2B_0} [C_1 f\nabla^2 f + 2C_2 (\nabla f)^2], \quad (8)$$

where

$$\begin{aligned} C_1 &= \frac{1}{2}(1 - \delta - \lambda) \\ C_2 &= \frac{1}{2}\left(\frac{1}{2} - \delta\right)\left(\frac{1}{2} - \lambda\right). \end{aligned} \quad (9)$$

### B. Application of the DDM formalism to the $\gamma$ -rigid Bohr Hamiltonian

We recall that the original Bohr Hamiltonian [1,2] is

$$H_B = -\frac{\hbar^2}{2B} \left[ \frac{1}{\beta^4} \frac{\partial}{\partial\beta} \beta^4 \frac{\partial}{\partial\beta} + \frac{1}{\beta^2 \sin 3\gamma} \frac{\partial}{\partial\gamma} \sin 3\gamma \frac{\partial}{\partial\gamma} - \frac{1}{4\beta^2} \sum_{k=1,2,3} \frac{Q_k^2}{\sin^2(\gamma - \frac{2}{3}\pi k)} \right] + V(\beta, \gamma), \quad (10)$$

where  $\beta$  and  $\gamma$  are the usual collective coordinates, while  $Q_k$  ( $k = 1, 2, 3$ ) are the components of angular momentum in the intrinsic frame, and  $B_0$  is the mass parameter, which is usually considered constant. The application of the DDM formalism in the case of X(3) symmetry leads to a Schrödinger equation as [31–33]

$$\begin{aligned} H\Psi(\beta, \theta, \phi) &= \left[ -\frac{\hbar^2}{2B_0} \left[ \frac{\sqrt{f}}{\beta^2} \frac{\partial}{\partial\beta} \beta^2 f \frac{\partial}{\partial\beta} \sqrt{f} + \frac{f^2}{3\beta^2} \Delta_\Omega \right] \right. \\ &\quad \left. + V_{\text{eff}}(\beta) \right] \Psi(\beta, \theta, \phi) = E\Psi(\beta, \theta, \phi), \end{aligned} \quad (11)$$

where  $\Delta_\Omega$  is the angular part of the Laplace operator given by

$$\Delta_\Omega = \frac{1}{\sin\theta} \frac{\partial}{\partial\theta} \sin\theta \frac{\partial}{\partial\theta} + \frac{1}{\sin^2\theta} \frac{\partial^2}{\partial\phi^2}. \quad (12)$$

In order to describe this situation with the Bohr Hamiltonian, the potential is assumed to be  $\gamma$  independent,  $V(\beta, \gamma) = U(\beta)$ , which allows the separation of the variables as

$$\Psi(\beta, \theta, \phi) = F(\beta)Y_{LM_L}(\theta, \phi). \quad (13)$$

Then, the radial equation is given by

$$\left[ -\frac{\hbar^2}{2B_0} \left[ \frac{\sqrt{f}}{\beta^2} \frac{\partial}{\partial\beta} \beta^2 f \frac{\partial}{\partial\beta} \sqrt{f} - \frac{L(L+1)f^2}{3\beta^2} \right] + V_{\text{eff}}(\beta) \right] F(\beta) = EF(\beta), \quad (14)$$

where  $L$  is the total angular momentum originating from the angular part of the wave function:

$$-\Delta_\Omega Y_{LM_L}(\theta, \phi) = L(L+1)Y_{LM_L}(\theta, \phi), \quad (15)$$

where  $Y_{LM_L}(\theta, \phi)$  are the spherical harmonics.

Equation (14) can be simplified by performing the derivations

$$\left[ -\frac{\hbar^2}{2B_0} \left[ \frac{d^2}{d\beta^2} + \frac{2}{\beta} \frac{d}{d\beta} - \frac{L(L+1)}{3\beta^2} \right] - \frac{\hbar^2}{2B_0} \left[ \frac{f'}{\beta f} + \left( \frac{f'}{2f} \right)^2 + \frac{2f'}{f} \frac{d}{d\beta} + \frac{f''}{2f} \right] + \frac{V_{\text{eff}}(\beta) - E}{f^2} \right] F(\beta) = 0. \quad (16)$$

The special form for the deformation function is

$$f(\beta) = 1 + \tau g(\beta), \quad \tau \ll 1, \quad (17)$$

where  $\tau$  is the DDM parameter. Note that this choice is made in order to have the same asymptotic behavior at the infinity as that of the sextic potential (1). Using this form for the deformation function in Eq. (16), one obtains

$$\left[ -\frac{\hbar^2}{2B_0} \left[ \frac{d^2}{d\beta^2} + \frac{2}{\beta} \frac{d}{d\beta} - \frac{L(L+1)}{3\beta^2} \right] + \bar{K}(E, \beta) \right] \times F(\beta) = 0, \quad (18)$$

where

$$\bar{K}(E, \beta) = -\frac{\hbar^2}{2B_0} \left[ \frac{\tau g'}{\beta(1+\tau g)} + \left( \frac{\tau g'}{2(1+\tau g)} \right)^2 + \frac{2\tau g'}{1+\tau g} \frac{d}{d\beta} + \frac{\tau g''}{2(1+\tau g)} \right] + \frac{V_{\text{eff}}(\beta) - E}{(1+\tau g)^2}. \quad (19)$$

Note that Eq. (18) is a complex differential equation. In order to find an approximate solution for it, it is convenient to expand Eq. (19) in power series of  $\tau$ . This approximation is good, even excellent owing to the smallness of the parameter  $\tau$ .

Then, Eq. (18) becomes

$$[H_\beta^{(0)} + H_\beta^{(p)}]F(\beta) = EF(\beta), \quad (20)$$

where  $H_\beta^{(0)}$  and  $H_\beta^{(p)}$  are the unperturbed and perturbed Hamiltonians, respectively given by

$$H_\beta^{(0)} = -\frac{\hbar^2}{2B_0} \left[ \frac{d^2}{d\beta^2} + \frac{2}{\beta} \frac{d}{d\beta} - \frac{L(L+1)}{3\beta^2} \right] + V(\beta) \quad (21)$$

and

$$H_\beta^{(p)} = \tau \frac{\hbar^2}{2B_0} \left[ C_1 \frac{(2g' + \beta g'')}{\beta} + \frac{4B_0 g}{\hbar^2} (E - V(\beta)) - 2g' \frac{d}{d\beta} - \frac{g'}{\beta} - \frac{g''}{2} \right]. \quad (22)$$

In this paper we define  $g(\beta)$  as

$$g(\beta) = a^{\frac{1}{2}} \beta^2 + a\beta^4 + a^{\frac{3}{2}} \beta^6, \quad (23)$$

where  $a$  is the same parameter of the potential (1). This choice will be justified later.

By substituting  $g(\beta)$  into the perturbed Hamiltonian and collecting the same powers of  $\beta$  we obtain

$$H_\beta^{(p)} = \tau \frac{\hbar^2}{2B_0} \left[ (-12a^{\frac{3}{2}} \beta^5 - 8a\beta^3 - 4a^{\frac{1}{2}} \beta) \frac{d}{d\beta} + \frac{4B}{\hbar^2} a^{\frac{3}{2}} (E - V(\beta)) \beta^6 + \left( \frac{4B}{\hbar^2} a (E - V(\beta)) + a^{\frac{3}{2}} (42C_1 - 21) \right) \beta^4 + \left( \frac{4B}{\hbar^2} a^{\frac{1}{2}} (E - V(\beta)) + a(20C_1 - 10) \right) \beta^2 + a^{\frac{1}{2}} (6C_1 - 3) \right]. \quad (24)$$

### C. Solutions of the $\beta$ equation for $\tau = 0$ within QES

In this subsection, we are interested in finding the eigenvalues and eigenvectors of the Hamiltonian (21) in the constant mass case. For this purpose, it is noteworthy to bring Eq. (20) to a Schrödinger form. This is easily achieved by changing the unperturbed wave function with  $F^{(0)}(\beta) = \frac{\xi^{(0)}(\beta)}{\beta}$ :

$$\left[ -\frac{d^2}{d\beta^2} + \frac{L(L+1)}{3\beta^2} + v(\beta) \right] \xi^{(0)}(\beta) = \varepsilon \xi^{(0)}(\beta), \quad (25)$$

with

$$\varepsilon = \frac{2B_0}{\hbar^2} E^{(0)}, \quad v(\beta) = \frac{2B_0}{\hbar^2} V(\beta). \quad (26)$$

The solution of this equation has been elaborated in detail in Refs. [21–24,28]. Here we will simply summarize that study by stating its main results which will of course help us in our present paper.

First, the comparison between Eq. (25) with that of the exactly solvable case of the sextic potential [23] leads to the following correspondences:

$$\left( 2s - \frac{1}{2} \right) \left( 2s - \frac{3}{2} \right) = \frac{L(L+1)}{3}, \quad (27)$$

$$v(\beta) = \left[ b^2 - 4a \left( s + \frac{1}{2} + M' \right) \right] \beta^2 + 2ab\beta^4 + a^2\beta^6. \quad (28)$$

The potential (28) is dependent on two parameters,  $a$  and  $b$ , and on the  $L$  quantum number through  $s$ .  $M'$  is a natural number which fixes the number of states that can be determined. This implication will be explained later in the discussion of the wave functions. The number of parameters is brought down to 1 by changing the variable with  $\beta = ya^{\frac{1}{4}}$ . Then by inserting the notations  $\varrho = \frac{b}{\sqrt{a}}$  and  $\varepsilon_y = \varepsilon/\sqrt{a}$  one gets

$$\left[ -\frac{d^2}{dy^2} + \frac{L(L+1)}{3y^2} + (\varrho^2 - 4c)y^2 + 2\varrho y^4 + y^6 \right] \eta^{(0)}(y) = \varepsilon_y \eta^{(0)}(y), \quad (29)$$

where

$$c = s + \frac{1}{2} + M'. \quad (30)$$

Because  $s$  depends on  $L$ , the potential of Eq. (29) is state dependent. Then  $s$  is given by

$$s(L) = \frac{1}{2} \left[ 1 + \sqrt{\frac{L(L+1)}{3} + \frac{1}{4}} \right]. \quad (31)$$

For  $L = 0$  and  $2$  the expression of  $s$  reduces to a simpler form:

$$s'(L) = \frac{L+3}{4}. \quad (32)$$

The condition (30) becomes

$$c = M' + \frac{L}{4} + \frac{5}{4} = \text{const.} \quad (33)$$

It can be easily checked that the above condition is satisfied if  $M'$  is decreased with one unit when  $L$  is increased with four. This means that for  $\frac{L}{2}$  even and  $\frac{L}{2}$  odd there are two different constants  $c$  [21]:

$$\begin{aligned} (M', L) &: (k, 0), (k-1, 4), (k-2, 8) \dots \\ &\Rightarrow k + \frac{5}{4} = c_0^{(k)}, \end{aligned} \quad (34)$$

$$\begin{aligned} (M', L) &: (k, 2), (k-1, 6), (k-2, 10) \dots \\ &\Rightarrow k + \frac{7}{4} = c_2^{(k)}, \end{aligned} \quad (35)$$

which differ from each other just by  $\frac{1}{2}$ . It is worth noting that the value of  $k = M'_{\text{max}}$  puts a limit on the number of states that could be determined and is called the QES order.

As an example, if  $k = 2$ , the highest angular momentum state that could be described analytically would be the state  $L = 10$ , while for  $k = 4$  it is the  $L = 18$  state, and so on.

This is actually a direct consequence of the condition (33). In the case of  $L > 2$ ,  $s$  becomes irrational so that Eq. (29) can no longer be solved for the  $M'$  integer and with the constant potential condition satisfied.

A possible way to handle this problem is to extract from the centrifugal term the quantity  $\frac{1}{y^2} \frac{L}{6} (\frac{L}{2} - 1)$ , and to replace  $y^2$  with its average  $\langle y^2 \rangle$  on  $\eta^0(y)$  eigenstates of the remaining Hamiltonian for each angular momentum  $L$ . With this approximation,  $s$  and  $c$  will have the same expressions as in Eqs. (32) and (33).

The constant potential condition is then exactly fulfilled for two distinct sets of states, corresponding to slightly different potentials. This picture is improved by considering the following form for the general potential:

$$v_m^{(k)}(y) = (\varrho^2 - 4c_m^{(k)})y^2 + 2\varrho y^4 + y^6 + u_m^{(k)}(\varrho) \quad m = 0, 2. \quad (36)$$

For a fixed  $k$ ,  $u_m^{(k)}$  are constants depending on  $\varrho$ , which are fixed such that the minimum energies of the potentials  $v_m^{(k)}$  are the same. Choosing  $u_0^{(k)} = 0$ , the other constant  $u_2^{(k)}$  is given by

$$u_2^{(k)}(\varrho) = \begin{cases} (\varrho^2 - 4c_0^{(k)})(y_{0,0}^{(k)})^2 \\ -(\varrho^2 - 4c_2^{(k)})(y_{0,2}^{(k)})^2 \\ + 2\varrho[(y_{0,0}^{(k)})^4 - (y_{0,2}^{(k)})^4] \\ + [(y_{0,0}^{(k)})^6 - (y_{0,2}^{(k)})^6] & \text{if } \varrho^2 < 4c_0^{(k)} \\ -(\varrho^2 - 4c_2^{(k)})(y_{0,2}^{(k)})^2 \\ - 2b(y_{0,2}^{(k)})^4 - (y_{0,2}^{(k)})^6 & \text{if } 4c_0^{(k)} < \varrho^2 < 4c_2^{(k)} \\ 0 & \text{if } \varrho^2 > 4c_2^{(k)} \end{cases} \quad (37)$$

where

$$(y_{0,m}^{(k)})^2 = \frac{1}{3}(-2\varrho + \sqrt{\varrho^2 + 12c_m^{(k)}}), \quad m = 0, 2 \quad (38)$$

are the absolute potential minima of the even  $\frac{L}{2}$  and odd  $\frac{L}{2}$  potentials. The shape of potential depends on the signs of  $\varrho^2 - 4c_m^{(k)}$  and  $\varrho$ . Indeed, when  $\varrho^2 > 4ac_m^{(k)}$ , the potential has a minimum at  $y = 0$  (spherical minimum) and it increases monotonously with  $y$ . However, when  $4c_0^{(k)} < \varrho^2 < 4c_2^{(k)}$ , it has a spherical and deformed minimum given by  $y_{0,m}^{(k)} = 0$  and  $y_{0,2}^{(k)} > 0$ , respectively. Finally, for  $\varrho^2 < 4c_0^{(k)}$ , the potential has a maximum and a minimum.

All these constants are taken into consideration in the fit of experimental data. Taking the ansatz function [21]

$$n_{n_\beta, L}^{(0)}(y) = N_{n_\beta, L} P_{n_\beta, L}^{(M')}(y^2) y^{\frac{L}{2}+1} e^{-\frac{y^4}{4} - \frac{\varrho y^2}{2}}, \quad n_\beta = 0, 1, 2, \quad (39)$$

Eq. (29) is then reduced to the following differential equation:

$$\begin{aligned} &\left[ -\left( \frac{d^2}{dy^2} + \frac{4s' - 1}{y} \frac{d}{dy} \right) + 2\varrho \frac{d}{dy} \right] P_{n_\beta, L}^{(M')}(y^2) \\ &+ 2y^2 \left( y \frac{d}{dy} - 2M' \right) P_{n_\beta, L}^{(M')}(y^2) = \lambda P_{n_\beta, L}^{(M')}(y^2), \end{aligned} \quad (40)$$

where  $P^{(M')}(y^2)$  is a polynomial in  $y^2$  of degree  $M'$ , while  $N_{n_\beta, L}$  are the normalization factors.

The eigenvalues  $\lambda^{(M')}$  are derived for each  $M'$  by the analytical procedure given in the Appendix of Refs. [21,34]. For any given value of  $M'$ , there are  $M' + 1$  solutions which are differentiated by the vibrational quantum number  $n_\beta$  in the following way: The smallest eigenvalue  $\lambda$  is corresponding to  $n_\beta = 0$ , while the highest is  $n_\beta = M' + 1$ .

For the present physical problem, we will only consider solutions with  $n_\beta = 0$ ,  $n_\beta = 1$ , and  $n_\beta = 2$ , corresponding to the ground, first, and second  $\beta$  bands, respectively.  $\lambda$  also

depends on  $L$  via  $s'$  and we must recall that at this point  $L$  and  $M'$  are interdependent via the condition (33), the actual relationship being dictated by the value of  $k$ . Therefore, the indexing of  $M'$  by  $\lambda$  will be replaced from here by  $k$ .

After all the algebraic manipulations that lead to Eq. (40) and taking into account the above considerations,  $\lambda$  can be alternatively given as the following:

$$\lambda = \lambda_{n_\beta, L}^{(k)}(\varrho) = \varepsilon_y - 4\varrho s' - u_m^{(k)}(\varrho) - \frac{1}{\langle y^2 \rangle_{n_\beta, L}} \frac{L}{6} \left( \frac{L}{2} - 1 \right). \quad (41)$$

From the above relation one finally extracts the total energy of the system in the case of  $\tau = 0$ :

$$E_{n_\beta, L}^{(0)} = \frac{\hbar^2 \sqrt{a}}{2B_0} \left[ \lambda_{n_\beta, L}^{(k)}(\varrho) + \varrho(L+3) + u_m^{(k)}(\varrho) + \frac{1}{\langle y^2 \rangle_{n_\beta, L}} \frac{L}{6} \left( \frac{L}{2} - 1 \right) \right], \quad (42)$$

which is indexed by the  $\beta$  vibration  $n_\beta$ , and also by the intrinsic angular momentum  $L$ . The index  $m$  is fully determined only by  $L$ .

Furthermore, the above energy also depends on the integer QES order  $k$ . As with the eigenvalue  $\lambda$ , the corresponding eigenfunctions of Eq. (40) are also dependent on  $k$  and  $L$ .

#### D. Solutions of the radial equation in the DDM case by QPM

Owing to the smallness of the DDM parameter  $\tau$ , it is therefore necessary to use the quantum mechanical perturbation theory. Hence, the first-order correction to the energy is given by [35]

$$E_{n_\beta, L}^{\text{corr}} = E_{n_\beta, L}^0 + \Delta E_{n_\beta, L}, \quad (43)$$

where  $E_{n_\beta, L}^0$  given in Eq. (42) are the unperturbed levels corresponding to the eigenfunctions solutions of the Schrödinger equation for  $\tau = 0$  and  $\Delta E_{n_\beta, L}$  is the correction induced by the DDM, given by

$$\Delta E_{n_\beta, L} = \tau \frac{\hbar^2}{2B_0} \langle \xi_{n_\beta, L}^{(M,0)}(\beta) | W | \xi_{n_\beta, L}^{(M,0)}(\beta) \rangle, \quad (44)$$

where

$$W = \left[ (-12a^{\frac{3}{2}}\beta^5 - 8a\beta^3 - 4a^{\frac{1}{2}}\beta) \frac{d}{d\beta} + \frac{4B}{\hbar^2} a^{\frac{3}{2}} (E - V(\beta)) \beta^6 + \left( \frac{4B}{\hbar^2} a (E - V(\beta)) + a^{\frac{3}{2}} (42C_1 - 21) \right) \beta^4 + \left( \frac{4B}{\hbar^2} a^{\frac{1}{2}} (E - V(\beta)) + a(20C_1 - 10) \right) \beta^2 + a^{\frac{1}{2}} (6C_1 - 3) \right]. \quad (45)$$

After substituting the sextic potential (36) into Eq. (45) and using the change of variable  $\beta = ya^{-1/4}$ , one obtains

$$\begin{aligned} \Delta E_{n_\beta, L} = & -2\tau \sqrt{a} \frac{\hbar^2}{B_0} \left[ \overline{(6y^5 + 4y^3 + 2y) \frac{d}{dy} + y^{12}} \right. \\ & + (1 + 2\varrho) y^{10} + (1 + 2\varrho + A_m^{(k)}) y^8 \\ & + (2\varrho + A_m^{(k)} - \varsigma_{n_\beta, L}^{(0)}) y^6 \\ & + \left. \left( (A_m^{(k)} - \varsigma_{n_\beta, L}^{(0)} - 21C_1 + \frac{21}{2}) y^4 \right. \right. \\ & \left. \left. + (5 - \varsigma_{n_\beta, L}^{(0)} - 10C_1) y^2 + \frac{3}{2} - 3C_1 \right] \right], \quad (46) \end{aligned}$$

where  $A_m^{(k)} = (\varrho^2 - 4c_m^{(k)})$ ,  $\varsigma_{n_\beta, L}^{(0)} = \lambda_{n_\beta, L}^{(k)}(\varrho) + \varrho(L+3) + \frac{1}{\langle y^2 \rangle_{n_\beta, L}} \frac{L}{6} \left( \frac{L}{2} - 1 \right)$ ,  $\overline{y^t}$  ( $t = 2, 4, 6, 8, 12$ ) are the mean values of  $y^t$  given by

$$\overline{y^t} = \int_0^\infty \eta_{n_\beta, L}^{(0)}(y) y^t \eta_{n_\beta, L}^{(0)}(y) dy, \quad (47)$$

and  $\overline{(6y^5 + 4y^3 + 2y) \frac{d}{dy}}$  is given by

$$\begin{aligned} \overline{(6y^5 + 4y^3 + 2y) \frac{d}{dy}} = & \int_0^\infty \eta_{n_\beta, L}^{(0)}(y) (6y^5 + 4y^3 + 2y) \\ & \times \frac{d}{dy} \eta_{n_\beta, L}^{(0)}(y) dy. \quad (48) \end{aligned}$$

It is clear that the expansion of  $W$  is given as polynomials in  $\beta$ , and then its mean value is calculated using the following integral [36]:

$$\begin{aligned} & \int_0^{+\infty} y^t e^{-(\frac{y^4}{2} + \varrho y^2)} dy \\ & = \frac{1}{2} \Gamma\left(\frac{t+1}{2}\right) 2^{-\frac{t+1}{4}} U\left(\frac{t+1}{4}; \frac{1}{2}; \frac{\varrho^2}{2}\right), \quad (49) \end{aligned}$$

where  $U\left(\frac{t+1}{4}; \frac{1}{2}; \frac{b^2}{2a}\right)$  are Kummer's functions which can be expressed in terms of the usual confluent hypergeometric functions as in Ref. [37]:

$$\begin{aligned} U\left(s, \frac{1}{2}, z\right) = & \frac{\pi^{1/2}}{\Gamma(s + \frac{1}{2})} F_1\left(s, \frac{1}{2}; z\right) - \frac{2\pi^{1/2}}{\Gamma(s)} \\ & \times F_1\left(s + \frac{1}{2}, \frac{3}{2}; z\right). \quad (50) \end{aligned}$$

Using the same method (QPM), the first-order correction to the eigenstate is given by [35]

$$\begin{aligned} \eta_{n_\beta, L}^{\text{corr}}(y) = & \eta_{n_\beta, L}^{(0)}(y) + \sum_{k \neq n_\beta} \left[ \frac{\int_0^\infty \eta_{k, L}^{(0)}(y) \vartheta \eta_{n_\beta, L}^{(0)}(y) dy}{\varsigma_{n_\beta, L}^{(0)} - \varsigma_{k, L}^{(0)}} \right] \\ & \times \eta_{k, L}^{(0)}(y), \quad (51) \end{aligned}$$

where

$$\begin{aligned}
\vartheta &= \vartheta(n_\beta, \varrho, \tau, \varsigma_{n_\beta, L}^{(0)}, A_m^{(k)}) \\
&= -2\tau\sqrt{a}\frac{\hbar^2}{B_0}\left[(6y^5 + 4y^3 + 2y)\frac{d}{dy}\right. \\
&\quad + (1 + 2\varrho)y^{10} + (1 + 2\varrho + A_m^{(k)})y^8 \\
&\quad + y^{12} + (2\varrho + A_m^{(k)} - \varsigma_{n_\beta, L}^{(0)})y^6 \\
&\quad + \left.\left((A_m^{(k)} - \varsigma_{n_\beta, L}^{(0)} - 21C_1 + \frac{21}{2})y^4\right.\right. \\
&\quad \left.\left.+ (5 - \varsigma_{n_\beta, L}^{(0)} - 10C_1)y^2 + \frac{3}{2} - 3C_1\right)\right]. \quad (52)
\end{aligned}$$

In a similar context, the probability density distribution can also be evaluated by the formula below:

$$\rho_{n_\beta, L}^{\text{corr}}(\beta) = \beta^2 |F_{n_\beta, L}^{\text{corr}}(\beta)|^2 = a^{-1/2} y^2 |\eta_{n_\beta, L}^{\text{corr}}(y)|^2. \quad (53)$$

### E. $B(E2)$ transition rates

Having the corrected eigenstate, we can also deduce the expression of the total wave function of the system:

$$\begin{aligned}
\Psi^{(\text{corr})}(\beta, \theta, \phi) &= F_{n_\beta, L}^{(\text{corr})}(\beta) Y_{LM_L}(\theta, \phi) \\
&= \frac{\xi_{n_\beta, L}^{(\text{corr})}(\beta)}{\beta} Y_{LM_L}(\theta, \phi). \quad (54)
\end{aligned}$$

The electromagnetic characteristics are investigated by the  $B(E2)$  transitions which are determined with the help of the transition operator:

$$\begin{aligned}
T_\mu^{(E2)} &= t\beta \left[ D_{\mu, 0}^2(\Omega) \cos \gamma + \frac{1}{\sqrt{2}} [D_{\mu, 2}^{2*}(\Omega) \right. \\
&\quad \left. + D_{\mu, -2}^2(\Omega)] \sin \gamma \right], \quad (55)
\end{aligned}$$

where  $D_{\mu, \mu'}^L(\Omega)$  are the Wigner functions of angular momentum  $L$ , and its projections  $\mu$  and  $\mu'$  on the body-fixed and laboratory-fixed  $z$  axis, respectively, while  $\Omega$  denotes the Euler angles and  $t$  is a scale factor. For  $\gamma = 0$  the quadrupole operator becomes [38]

$$T_\mu^{(E2)} = t\beta \sqrt{\frac{4\pi}{5}} Y_{2\mu}(\theta, \phi). \quad (56)$$

The  $B(E2)$  transition rates from an initial to a final state are given by

$$B(E2; n_\beta L \rightarrow n'_\beta L') = \frac{1}{2L+1} |(n'_\beta L' || T^{(E2)} || n_\beta L)|^2. \quad (57)$$

These physical quantities are calculated using the wave functions of Eq. (51) and the volume element  $dV = \beta^2 \sin \theta d\beta d\theta d\phi = a^{-3/4} y^2 \sin \theta dy d\theta d\phi$ . Therefore, the final expression of the reduced  $B(E2)$  transition probabilities, normalized to the transition from the first excited state to the

ground state (g.s.), is given by

$$\begin{aligned}
B(E2) &= T_{n_\beta, L, n'_\beta, L'} = \frac{B(E2; n_\beta; L \rightarrow n'_\beta, L')}{B(E2; 0; 2 \rightarrow 0, 0)} \\
&= \left( \frac{C_{0,0,0}^{L2L'} I_{n_\beta, L, n'_\beta, L'}^{\text{corr}}}{C_{0,0,0}^{220} I_{0,2,0,0}^{\text{corr}}} \right)^2, \quad (58)
\end{aligned}$$

where the radial matrix elements  $I_{n_\beta, L, n'_\beta, L'}^{\text{corr}}$  can be given either in  $\beta$  or  $y$  variable:

$$\begin{aligned}
I_{n_\beta, L, n'_\beta, L'}^{\text{corr}} &= \int_0^{+\infty} F_{n_\beta, L}^{\text{corr}}(\beta) \beta F_{n'_\beta, L'}^{\text{corr}}(\beta) \beta^2 d\beta \\
&\quad \times a^{-1/4} \int_0^{+\infty} \eta_{n_\beta, L}^{\text{corr}}(y) y \eta_{n'_\beta, L'}^{\text{corr}}(\beta) dy, \quad (59)
\end{aligned}$$

calculated as in Refs. [36,37]. Having the corrected wave function and energy spectrum, we are in a position to examine the results in the next section.

## III. NUMERICAL RESULTS AND DISCUSSION

This section is divided into five subsections. In the first one, we will present some theoretical aspects of the DDM concept within the  $X(3)$  model under the sextic potential. In the second one, we will analyze the obtained spectra for different nuclei, and in the third subsection we will deal with transition probabilities. The correlation between the minimal length (ML) and the DDM will be investigated in the fourth subsection, and finally, in the fifth subsection, we reveal the DDM effect on the variation of the moment of inertia of the ground state band.

### A. Theoretical aspects of the DDM parameter for $X(3)$ -sextic

The elaborated model dubbed  $X(3)$ -SDDMA was applied to study collective excited states of several  $\gamma$ -rigid nuclei for which the parameter  $\gamma$  is fixed to  $\gamma = 0$ . The theoretical predictions are done with Eq. (43) for low-lying bands which are classified by the principal quantum number  $n_\beta$ : the g.s. band with  $n_\beta = 0$ , the first  $\beta$  band with  $n_\beta = 1$ , and the second  $\beta$  band with  $n_\beta = 2$ . Moreover, due to the  $\gamma$  rigidity there is no  $\gamma$  band in the present solution.

Before dealing with the theoretical aspects of the present model, several remarks need to be made. First of all, the choice of the function  $g(\beta)$  in Eq. (23) is made in order to maintain the scaling property [21] given by

$$E_{n_\beta, L}^{\text{corr}}(a, b, \tau) = \sqrt{a} E_{n_\beta, L}^{\text{corr}}(\varrho, \tau), \quad (60)$$

where  $\varrho = \frac{b}{\sqrt{a}}$ .

On the other hand, the choice of the ambiguity parameters  $\lambda$ ,  $\delta$ , and  $\kappa$  leads to different Hamiltonians (4) and eventually to different eigenvalue problems. In the present paper we restrict our study to BenDaniel and Duke [39], where  $\lambda = \delta = 0$  (i.e.,  $C_1 = \frac{1}{2}$ ).

We should notice here that, in order to investigate the DDM effect on the energy spectra and  $B(E2)$  transition rates, the same QES order ( $k = 2$ ) has been used as in Ref. [21]. Thus, the index  $k$  will be dropped as it has a fixed value. The benefit

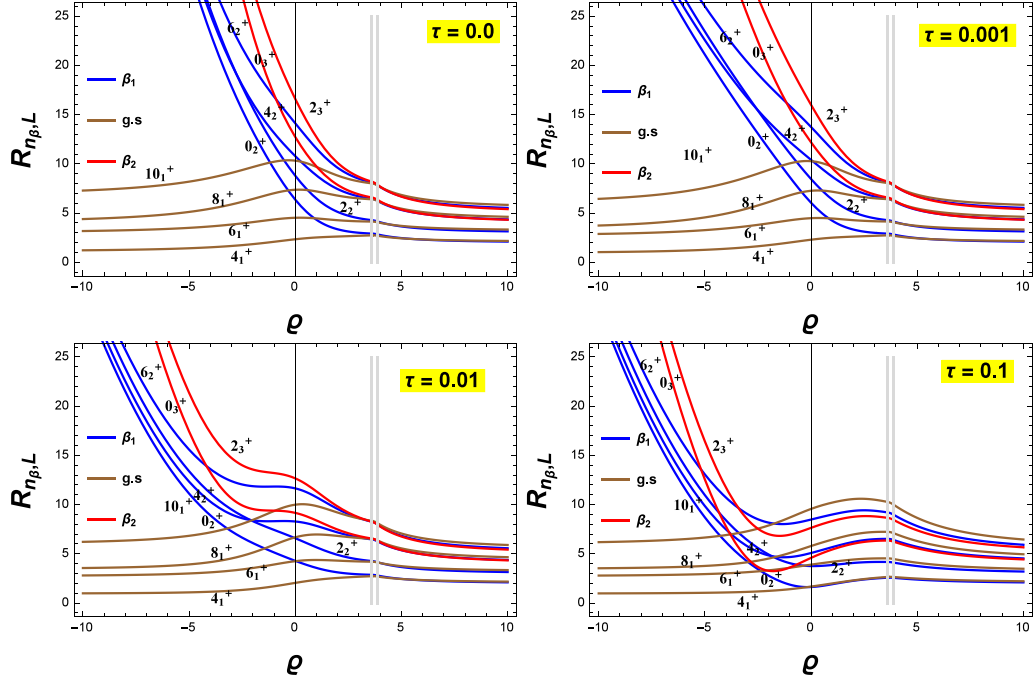


FIG. 1. Energy spectra of the ground state band and of the first two  $\beta$  bands, given by Eq. (61), are plotted as a function of the parameter  $\varrho$  for  $\tau = 0, 0.001, 0.01, 0.1$  and  $k = 2$ . The energy lines are indexed by  $L_{n_\beta+1}^+$ , where  $n_\beta = 0$  for the ground state band,  $n_\beta = 1$  for the first  $\beta$  band, and  $n_\beta = 2$  for the second  $\beta$  band.

of the  $k = 2$  case is that explicit analytical expressions for the energies and wave functions are still possible and are detailed in the Appendix of Ref. [21].

The results for  $k > 2$  are considered without any problem in Ref. [34], where the  $\gamma$ -rigid Bohr Hamiltonian with anharmonic sextic oscillator potential in the constant mass case has been extensively studied; also, the evolution of the spectral and electromagnetic properties by considering higher exact solvability orders ( $k > 2$ ) is investigated.

As mentioned in Ref. [34], for  $k = 2$ , one can describe states up to  $L = 10^+$  in the g.s. band, up to  $L = 6^+$  in the first  $\beta$  band, and up to  $L = 2^+$  in the second  $\beta$  band.

From Eq. (43) one can see that the energy spectrum normalized to the energy of the first excited state depends only on two free parameters  $\varrho$  and  $\tau$ . However, here one has to notice that the DDM parameter  $\tau$  should not be regarded as a simple additional one for fitting experimental data, but as a model's structural one, where it is connected to the space curvature based on the use of deformed canonical commutation relations as it has been shown in Refs. [15,40].

Another important aspect of the DDM approach is the physical meaning of the DDM parameter. Such a study has been extensively conducted in Ref. [41], where the comparison of the DDM Bohr Hamiltonian to the five-dimensional (5D) classical limit of Hamiltonians of the six-dimensional (6D) interacting boson model (IBM) shows that the DDM parameter is proportional to the strength of the pairing interaction in the  $U(5)$  (vibrational) symmetry limit, while it is proportional to the quadrupole-quadrupole interaction in the  $SU(3)$  (rotational) symmetry limit, and to the difference of the pairing interactions among  $s$  and  $d$  bosons and  $d$  bosons alone in the  $O(6)$  ( $\gamma$ -soft) limit. This connection has been

achieved using the coefficients of the term  $\frac{1}{\sin 3\gamma} \frac{\partial}{\partial \gamma} \sin 3\gamma \frac{\partial}{\partial \gamma}$  of Eqs. (8) and (34) of Ref. [41]. Moreover, for the present solution, which is a version of the critical symmetry  $X(5)$ , due to the  $\gamma$  rigidity, no terms of the form  $\frac{1}{\sin 3\gamma} \frac{\partial}{\partial \gamma} \sin 3\gamma \frac{\partial}{\partial \gamma}$  appear in Eq. (14). However, the comparison of the 5D DDM Bohr Hamiltonian with the sextic potential using the deformation function given in Eq. (17) to the 5D classical limit of Hamiltonians of the 6D IBM shows that the DDM parameter contains similar physical meaning as in Ref. [41]. The only noticeable difference is that the new DDM parameter is normalized by the factor  $a^{1/2}$ .

For further calculations one defines the energy ratios:

$$R_{n_\beta, L} = \frac{E_{n_\beta, L}^{\text{corr}} - E_{0,0}^{\text{corr}}}{E_{0,2}^{\text{corr}} - E_{0,0}^{\text{corr}}} \quad (61)$$

In order to reveal the DDM effect on the energy spectra, in this subsection we analyze the plot of energy ratios  $R_{n_\beta, L}$  given in Eq. (61) as a function of  $\varrho$  for  $\tau = 0, 0.001, 0.01, 0.1$  in Fig. 1. From this, we can make some useful remarks: By varying the potential parameter  $\varrho$  from the large values to a null one ( $\varrho = 0$ ),  $X(3)$ -SDDMA covers a shape phase transition from a  $\gamma$ -rigid prolate harmonic vibrator to an anharmonic one. Hence, our analysis is carried out for three regions, namely, the spherical, deformed, and critical point ones. For  $\varrho \rightarrow +\infty$ ,  $X(3)$ -SDDMA reproduces the results of the  $\gamma$ -rigid prolate harmonic vibrator called  $X(3)$ - $\beta^2$  [42]; the supplementary effect of the DDM parameter in this region hints at the fact that the energy spectra are displaced to higher values in comparison with  $\tau = 0$ . In the intervals  $[2\sqrt{c_0^{(2)}}, 2\sqrt{c_2^{(2)}}]$ , one observes a kink in the energy curves

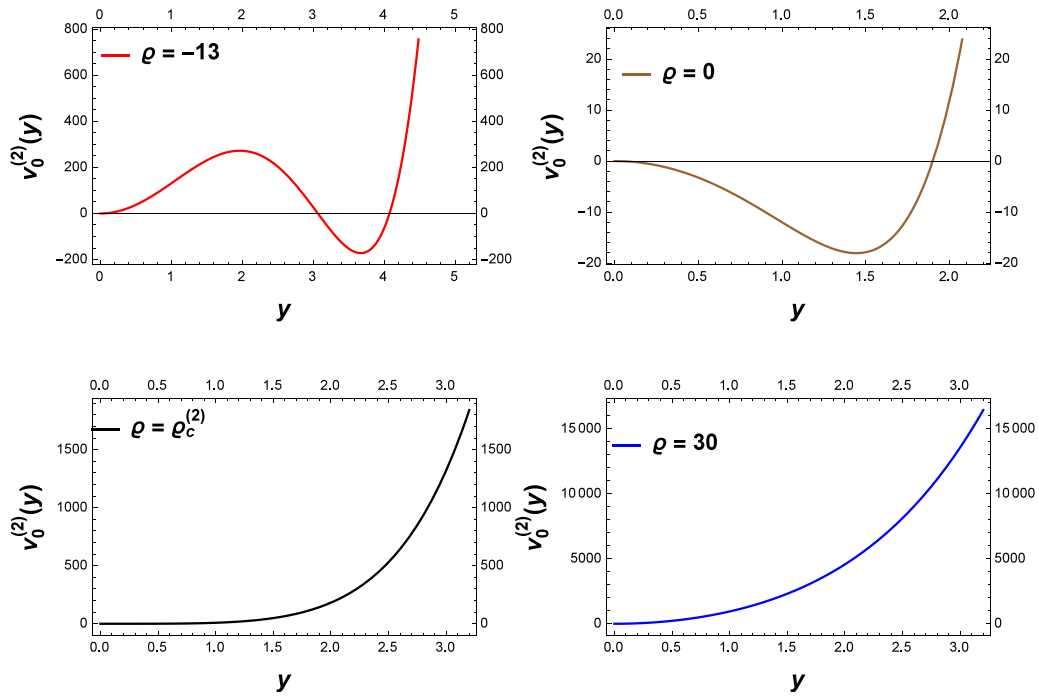


FIG. 2. Shape evolution of the sextic potential  $v_0^{(2)}(y)$ , given by Eq. (36), as a function of the parameter  $\varrho$  for  $c_0^{(2)} = \frac{13}{4}$  and  $u_0^{(2)} = 0$ .

which happens at a critical value  $\varrho_c^{(2)}$ . This value corresponds to the absolute maximum of the signature ratio  $R_{4,2}$  and is interpreted as the critical point for a first order shape phase transition between a  $\gamma$ -rigid prolate harmonic vibrator (spherical shape) and a  $\gamma$ -rigid prolate anharmonic vibrator (deformed shape) in the framework of the presently adopted sextic potential. By continuously varying the DDM parameter  $\tau$ , the critical point  $\varrho_c$  migrates to higher values of  $\varrho$ . Finally, in the deformed region (i.e.,  $\varrho < 2\sqrt{c_0^{(2)}}$ ), when  $\tau$  is increased, the two  $\beta$  bands go to infinity slowly. Also, local minima appear in the left side of  $\varrho = 0$ , while the ground state band energies maintain finite values.

As can be seen in Fig. 2, where some shapes of the energy potential given by Eq. (36) are plotted as a function of  $y$  for  $\varrho \in \{-13, -\varrho_c^{(2)}, \varrho_c^{(2)}, 30\}$ , the shape of the potential depends on  $\varrho$ . Indeed, for  $\varrho = -13$  ( $\alpha < -2\sqrt{c_0^{(2)}}$ ) two minima appear: a spherical and a deformed one, separated by a high barrier. Furthermore, for  $\varrho = -\varrho_c^{(2)}$  the potential has a single deformed minimum. Moreover, for  $\varrho = 30$  ( $\varrho \rightarrow +\infty$ ), the pure harmonic oscillator is reproduced. Finally, for  $\varrho = \varrho_c^{(2)}$  ( $\varrho \in [2\sqrt{c_0^{(2)}}, 2\sqrt{c_2^{(2)}}]$ ), as was explained in Ref. [21], it corresponds to the situation when the spherical and deformed minima of the potential energy are degenerated, where the potential shape is the flattest.

For the sake of revealing the DDM effect on the energy spectrum, in the context of  $\gamma$ -rigid nuclei, especially in the critical point  $\varrho^c$ , several energy ratios (61) and  $B(E2)$  (58) are presented in Fig. 3. from which one can draw some useful insights. First, the states are grouped two by two in each band. Furthermore, apart from  $4_{g.s.}^+$ ,  $0_{\beta_1}^+$ ,  $2_{\beta_1}^+$ , and  $0_{\beta_2}^+$ , which decrease with DDM parameter  $\tau$ , all the energy levels steadily increase

when  $\tau$  is raised. Another important aspect of the present paper is the specific spectral characteristics which must be studied when the mass parameter depends on the deformation coordinate. Here, one especially refers to the approximate degeneracy of states for different angular momenta ( $\Delta L = 4$ ) belonging to different bands in the case of  $\tau = 0$  [21,34]. Excepting the states  $4_{g.s.}^+$  and  $0_{\beta_1}^+$ , the DDM partially removes this approximate degeneracy. Concerning the  $B(E2)$  transition rates, apart from  $10_1 \rightarrow 8_1$ ,  $6_{\beta_1} \rightarrow 4_{\beta_1}$ , and  $2_{\beta_2} \rightarrow 0_{\beta_2}$  transitions, which increase with  $\tau$ , all the intraband transitions of the ground state and first two  $\beta$  bands are decreasing with  $\tau$ . In what concerns the relevant interband transitions, both from the first  $\beta$  band head to the first excited state and from the second  $\beta$  band to the first one, they are slowly decreasing with the change of  $\tau$  to higher values.

## B. Energy spectra

The numerical realization of this model consists in reproducing, with a good precision, the experimental data for energy spectra of the g.s. band and the first two  $\beta$  bands given by Eq. (61) and  $B(E2)$  transition rates for series of  $^{98-108}\text{Ru}$ ,  $^{100-102}\text{Mo}$ ,  $^{116-130}\text{Xe}$ ,  $^{180-196}\text{Pt}$ ,  $^{172}\text{Os}$ ,  $^{146-150}\text{Nd}$ ,  $^{132-134}\text{Ce}$ ,  $^{154}\text{Gd}$ ,  $^{156}\text{Dy}$ , and  $^{150-152}\text{Sm}$  isotopes with respect to  $X(3)$ -sextic [21] model predictions. This task is achieved through determination of the optimal values of the free model's parameters  $\varrho$  and  $\tau$  by making use of the quality measure

$$\sigma = \sqrt{\frac{\sum_{i=1}^{N'} (E_{n_{\beta},L}^i(\text{exp}) - E_{n_{\beta},L}^{\text{corr},i}(\text{th}))^2}{N'(E_{0,2})^2}}, \quad (62)$$



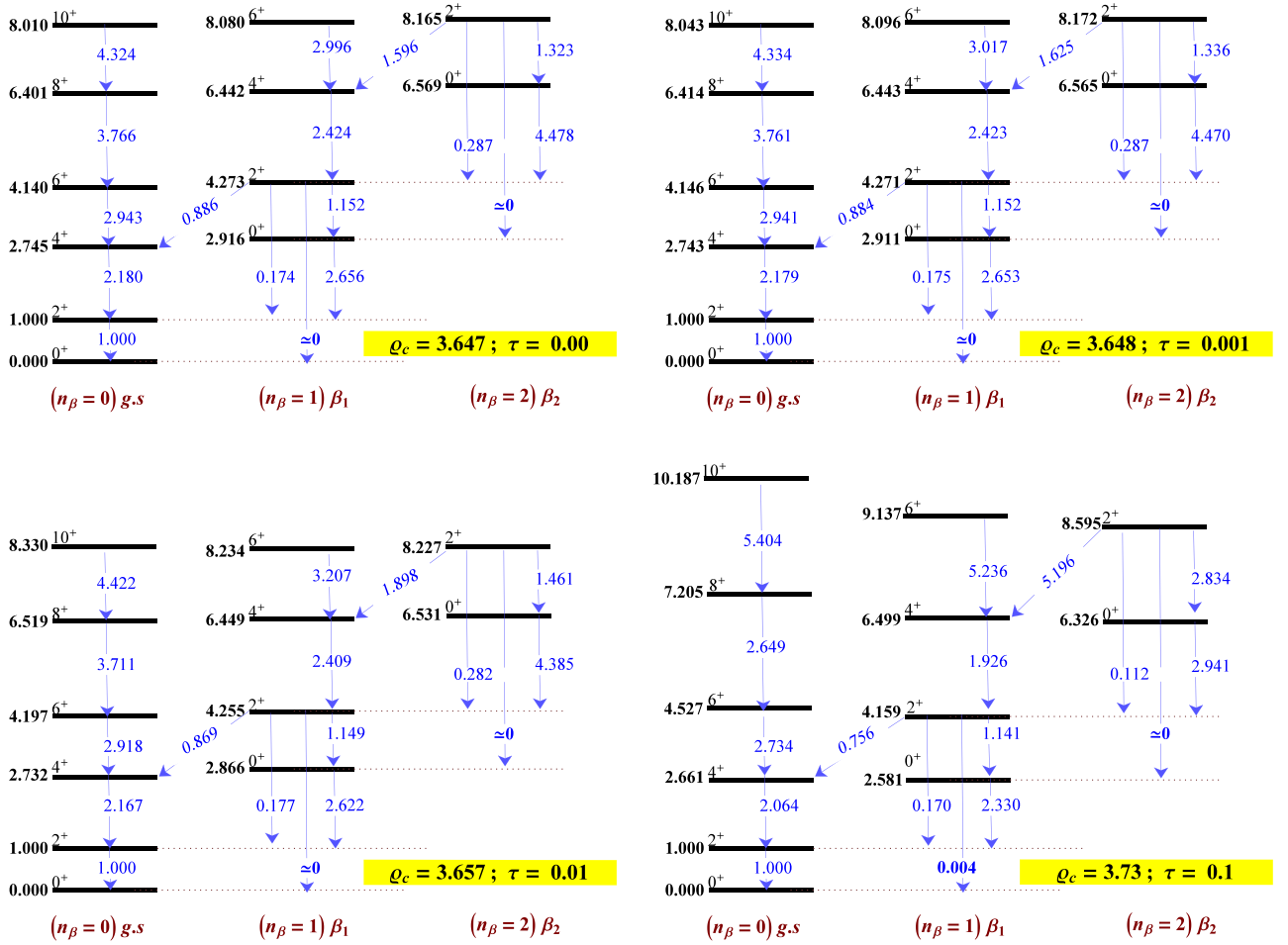


FIG. 3. Energy spectra (61) and  $B(E2)$  transitions (58) for the ground state band ( $n_\beta = 0$ ), the first  $\beta$  band ( $n_\beta = 1$ ), and the second  $\beta$  band ( $n_\beta = 2$ ) are visualized for  $(\rho_c, \tau) = (3.647, 0.00)$ ,  $(3.648, 0.001)$ ,  $(3.657, 0.01)$ , and  $(3.73, 0.1)$ .

where  $N'$  denotes the number of states, while  $E_{n_\beta, L}^i(\text{exp})$  and  $E_{n_\beta, L}^{\text{corr}, i}(\text{th})$  represent the experimental and theoretical energies of the  $i$ th level, respectively.  $E_{0,2}$  is the energy of the first excited level of the g.s. band.

Our theoretical results for 35 nuclei are shown in Tables I and II. In the same tables, we give also the experimental data and the numerical results of the constant mass case for the sextic potential  $[X(3)\text{-S}]$  [21]. All these data are fitted involving the two free parameters  $\rho$  and  $\tau$ . Their values and the corresponding rms are indicated in the same tables.

Based on these data, we see that the obtained results for the levels belonging to g.s., first, and second  $\beta$  bands are in a quite satisfactory agreement with experimental data for 74% of all studied nuclei. Indeed, the lowest  $\sigma$  value (0.07) is obtained for  $^{98}\text{Ru}$ . Moreover, the nuclei  $^{194}\text{Pt}$ ,  $^{102}\text{Mo}$ , and  $^{188}\text{Pt}$  have the  $\sigma$  values near to 0.10; further, the  $\sigma$  values of the nuclei  $^{118,122}\text{Xe}$ ,  $^{100-104}\text{Ru}$ ,  $^{134}\text{Ce}$ , and  $^{190,196}\text{Pt}$  are near 0.20; also, those of  $^{120}\text{Xe}$  and  $^{148}\text{Nd}$  are near 0.30. Additionally, those of  $^{126,130}\text{Xe}$ ,  $^{100}\text{Mo}$ ,  $^{132}\text{Ce}$ ,  $^{184}\text{Pt}$ , and  $^{150}\text{Sm}$  are near 0.40. Finally, those of  $^{116,124}\text{Xe}$ ,  $^{108}\text{Ru}$ ,  $^{172}\text{Os}$ ,  $^{180,182}\text{Pt}$ , and  $^{146}\text{Nd}$  are between 0.46 and 0.76.

On the other hand, the fitting quality of our results for all studied nuclei is better than that of the model  $X(3)\text{-S}$  [21] with respect to experimental data. This is explained by the fact that here the mass parameter depends on the  $\beta$  variable, while in Ref. [21] the mass is considered as a constant.

Also, as can be seen, there are some discrepancies in the ground state band of some isotopes like  $^{150}\text{Nd}$ ,  $^{152}\text{Sm}$ ,  $^{154}\text{Gd}$ , and  $^{156}\text{Dy}$ . These exceptions are not surprising, since these nuclei prefer a  $\gamma$ -stable structure. In other words, they are well described by the  $X(5)$  model, while the DDM improves slightly the  $\beta$  bands. For the nuclei  $^{128-130}\text{Xe}$  and  $^{192}\text{Pt}$ , the fitted values of  $\tau$  vanish. Physically speaking, these nuclei are pure vibrators.

Moreover, from Tables I and II, one can see that the g.s. and the  $\beta$  bands are more sensitive to the potential shapes. Indeed, for the nuclei situated in the spherical region ( $\rho > 2\sqrt{c_2^{(2)}}$ ), the g.s. band levels are well reproduced. Such a fact is well observed in the  $^{120-126}\text{Xe}$  isotopes. However, in the case of the deformed nuclei ( $\rho < 2\sqrt{c_0^{(2)}}$ ), the  $\beta$  band is well described, which is the case of the  $^{180-184}\text{Pt}$  isotopes.

TABLE I. Energy spectra for the ground state band and the first two  $\beta$  bands given by Eq. (61) are compared with the available experimental data [43–57] of the nuclei  $^{116-130}\text{Xe}$ ,  $^{100-102}\text{Mo}$ ,  $^{98-108}\text{Ru}$ , and  $^{132-134}\text{Ce}$  and with results available in Ref. [21]. In the first line of each nucleus are given the experimental data, in the second line are the corresponding  $X(3)\text{-S}$  [21], while in the third line are the corresponding  $X(3)\text{-SDDMA}$  for ( $\lambda = \delta = 0$ ). In brackets are indicated possible candidate energy states for the corresponding predicted data, which were not included in the fit.

Nucleus	$R_{0,4}$	$R_{0,6}$	$R_{0,8}$	$R_{0,10}$	$R_{1,0}$	$R_{1,2}$	$R_{1,4}$	$R_{1,6}$	$R_{2,0}$	$R_{2,2}$	$\sigma$	$\varrho$	$\tau$
$^{116}\text{Xe}$ Expt.	2.33	3.90	5.62	7.45		2.58	3.96	5.38					
$X(3)\text{-S}$	2.28	3.48	4.97	6.26	2.25	3.35	4.76	6.02	4.75	5.93	0.72	6.62	0.0
$X(3)\text{-SDDMA}$	2.21	3.46	4.90	6.34	2.11	3.20	4.51	5.86	4.43	5.63	0.64	9.79	0.075
$^{118}\text{Xe}$ Expt.	2.40	4.14	6.15	8.35	2.46	3.64	5.13		(5.10)				
$X(3)\text{-S}$	2.61	3.94	5.98	7.48	2.71	3.98	5.93	7.44	6.01	7.47	0.49	4.16	0.0
$X(3)\text{-SDDMA}$	2.47	4.01	6.11	8.27	2.39	3.72	5.60	7.56	5.48	7.20	0.19	5.08	0.080
$^{120}\text{Xe}$ Expt.	2.47	4.33	6.51	8.90	2.82	3.95	5.31		(6.93)				
$X(3)\text{-S}$	2.73	4.11	6.32	7.91	2.88	4.21	6.34	7.94	6.45	8.01	0.57	3.79	0.0
$X(3)\text{-SDDMA}$	2.52	4.15	6.42	8.82	2.43	3.83	5.84	8.00	5.70	7.58	0.27	4.70	0.091
$^{122}\text{Xe}$ Expt.	2.50	4.43	6.69	9.18	3.47	4.51			(7.63)				
$X(3)\text{-S}$	2.63	4.26	6.74	8.73	3.29	5.02	7.33	9.44	7.72	9.89	0.30	2.11	0.0
$X(3)\text{-SDDMA}$	2.57	4.30	6.79	9.11	3.06	4.79	7.06	9.38	7.32	9.58	0.22	2.16	0.011
$^{124}\text{Xe}$ Expt.	2.48	4.37	6.58	8.96	3.58	4.60	5.69		(6.70)	(7.63)			
$X(3)\text{-S}$	2.70	4.17	6.50	8.23	3.01	4.48	6.70	8.50	6.91	8.69	0.53	2.99	0.0
$X(3)\text{-SDDMA}$	2.70	4.26	6.66	8.79	2.75	4.17	6.37	8.38	6.37	8.20	0.46	3.81	0.032
$^{126}\text{Xe}$ Expt.	2.42	4.21	6.27	8.64	3.38	4.32	5.25		(6.57)				
$X(3)\text{-S}$	2.72	4.09	6.29	7.86	2.86	4.18	6.30	7.89	6.40	7.95	0.55	3.83	0.0
$X(3)\text{-SDDMA}$	2.57	4.11	6.34	8.47	2.55	3.92	5.94	7.91	5.88	7.64	0.45	4.34	0.049
$^{128}\text{Xe}$ Expt.	2.33	3.92	5.67		7.60	3.57	4.52			(5.87)			
$X(3)\text{-S}$	2.66	4.01	6.12	7.65	2.78	4.07	6.10	7.65	6.19	7.69	0.44	4.00	0.0
$X(3)\text{-SDDMA}$	2.66	4.01	6.12	7.65	2.78	4.07	6.10	7.65	6.19	7.69	0.44	4.00	0.0
$^{130}\text{Xe}$ Expt.	2.25	3.63	5.03		3.35	(4.01)	(4.53)						
$X(3)\text{-S}$	2.41	3.67	5.37	6.75	2.43	3.60	5.23	6.59	5.26	6.55	0.50	5.18	0.0
$X(3)\text{-SDDMA}$	2.41	3.67	5.37	6.75	2.43	3.60	5.23	6.59	5.26	6.55	0.50	5.18	0.0
$^{100}\text{Mo}$ Expt.	2.12	3.45	4.91	6.29	1.30	2.73							
$X(3)\text{-S}$	2.20	3.37	4.72	5.95	2.14	3.20	4.47	5.66	4.44	5.54	0.43	8.63	0.0
$X(3)\text{-SDDMA}$	2.20	3.45	4.89	6.34	2.09	3.18	4.49	5.83	4.39	5.89	0.37	10.40	0.090
$^{102}\text{Mo}$ Expt.	2.51	4.48	6.81	9.41	2.35	3.86							
$X(3)\text{-S}$	2.67	4.19	6.57	8.39	3.09	4.65	6.90	8.80	7.16	9.07	0.63	2.65	0.0
$X(3)\text{-SDDMA}$	2.61	4.35	6.83	9.45	2.55	4.04	6.23	8.59	6.10	8.14	0.13	4.09	0.084
$^{98}\text{Ru}$ Expt.	2.14	3.41	4.79	6.13	2.03								
$X(3)\text{-S}$	2.21	3.38	4.73	5.97	2.15	3.21	4.49	5.68	4.46	5.57	0.1	8.44	0.0
$X(3)\text{-SDDMA}$	2.16	3.37	4.69	6.03	2.05	3.10	4.31	5.56	4.22	5.34	0.07	14.09	0.100
$^{100}\text{Ru}$ Expt.	2.27	3.85	5.67	7.85	2.10								
$X(3)\text{-S}$	2.58	3.90	5.88	7.36	2.66	3.92	5.82	7.31	5.89	7.32	0.37	4.28	0.0
$X(3)\text{-SDDMA}$	2.42	3.84	5.75	7.60	2.36	3.61	5.36	7.07	5.28	6.82	0.18	5.40	0.053
$^{102}\text{Ru}$ Expt.	2.33	3.94	5.70	7.23	1.99								
$X(3)\text{-S}$	2.50	3.79	5.64	7.08	2.55	3.77	5.54	6.98	5.59	6.96	0.28	4.63	0.0
$X(3)\text{-SDDMA}$	2.43	3.80	5.66	7.36	2.40	3.63	5.36	6.97	5.32	6.79	0.21	5.21	0.03
$^{104}\text{Ru}$ Expt.	2.48	4.35	6.48	8.69	(2.76)	4.23	5.81						
$X(3)\text{-S}$	2.74	4.14	6.41	8.02	2.92	4.28	6.45	8.10	6.58	8.19	0.40	3.62	0.0
$X(3)\text{-SDDMA}$	2.58	4.17	6.46	8.71	2.55	3.94	6.01	8.08	5.93	7.76	0.16	4.30	0.058
$^{106}\text{Ru}$ Expt.	2.66	4.80	7.31	10.02	3.67								
$X(3)\text{-S}$	2.55	4.43	7.14	9.55	4.10	6.20	8.55	11.19	9.36	12.20	0.34	1.16	0.0
$X(3)\text{-SDDMA}$	2.41	4.40	7.04	9.81	3.81	5.93	8.16	11.03	8.83	11.80	0.27	0.98	0.006
$^{108}\text{Ru}$ Expt.	2.75	5.12	8.02	11.31	4.03								
$X(3)\text{-S}$	2.49	4.50	7.30	9.92	4.75	7.01	9.31	12.22	10.43	13.65	0.83	0.73	0.0
$X(3)\text{-SDDMA}$	2.38	4.45	7.16	10.01	4.50	6.76	8.93	11.79	9.93	13.20	0.80	0.61	0.003
$^{132}\text{Ce}$ Expt.	2.64	4.74	7.16	9.71	3.56	4.60	5.94						
$X(3)\text{-S}$	2.65	4.23	6.65	8.56	3.18	4.83	7.11	9.11	7.43	9.47	0.70	2.36	0.0
$X(3)\text{-SDDMA}$	2.68	4.43	7.00	9.65	2.67	4.20	6.50	8.90	6.41	8.52	0.45	3.63	0.063
$^{134}\text{Ce}$ Expt.	2.56	4.55	6.87	9.09	3.75	4.80							
$X(3)\text{-S}$	2.61	4.30	6.82	8.89	3.42	5.23	7.56	9.77	8.01	10.31	0.26	1.89	0.0
$X(3)\text{-SDDMA}$	2.58	4.31	6.84	9.05	3.33	5.14	7.46	9.76	7.86	10.21	0.24	1.87	0.003

TABLE II. Same as in Table I, but for the available experimental data [58–72] of the nuclei  $^{172}\text{Os}$ ,  $^{180-196}\text{Pt}$ ,  $^{146-148}\text{Nd}$ ,  $^{150-152}\text{Sm}$ ,  $^{154}\text{Gd}$ , and  $^{156}\text{Dy}$ .

Nucleus	$R_{0,4}$	$R_{0,6}$	$R_{0,8}$	$R_{0,10}$	$R_{1,0}$	$R_{1,2}$	$R_{1,4}$	$R_{1,6}$	$R_{2,0}$	$R_{2,2}$	$\sigma$	$\varrho$	$\tau$
$^{172}\text{Os}$ Expt.	2.66	4.63	6.70	8.89	3.33	3.56	5.00	6.81					
X(3)-S	2.65	4.00	6.10	7.63	2.77	4.06	6.07	7.62	6.16	7.66	0.77	4.02	0.0
X(3)-SDDMA	2.48	3.91	5.91	7.76	2.46	3.74	5.57	7.31	5.53	7.10	0.69	4.86	0.039
$^{180}\text{Pt}$ Expt.	2.68	4.94	7.71	10.93	3.12	5.62	8.15	10.77	(7.69)				
X(3)-S	2.56	4.40	7.07	9.41	3.92	5.96	8.32	10.86	9.03	11.75	0.69	1.31	0.0
X(3)-SDDMA	2.32	4.37	6.95	9.91	3.59	5.71	7.85	10.84	8.41	11.43	0.55	0.89	0.011
$^{182}\text{Pt}$ Expt.	2.71	5.00	7.78	10.96	3.22	5.53	8.00	10.64	(7.43)				
X(3)-S	2.57	4.40	7.05	9.37	3.88	5.90	8.26	10.77	8.95	11.64	0.72	1.35	0.0
X(3)-SDDMA	2.32	4.37	6.94	9.91	3.53	5.64	7.78	10.75	8.31	11.31	0.56	0.92	0.011
$^{184}\text{Pt}$ Expt.	2.67	4.90	7.55	10.47	3.02	5.18	7.57	11.04					
X(3)-S	2.57	4.38	7.01	9.29	3.79	5.77	8.13	10.59	8.77	11.39	0.65	1.44	0.0
X(3)-SDDMA	2.30	4.35	6.90	9.92	3.39	5.49	7.60	10.80	8.07	11.05	0.45	0.94	0.014
$^{186}\text{Pt}$ Expt.	2.56	4.58	7.01	9.70	2.46	4.17	6.38	8.36					
X(3)-S	2.68	4.18	6.53	8.30	3.04	4.56	6.80	8.64	7.03	8.87	0.62	2.82	0.0
X(3)-SDDMA	2.61	4.38	6.90	9.63	2.53	4.03	6.25	8.68	6.09	8.19	0.16	4.09	0.095
$^{188}\text{Pt}$ Expt.	2.53	4.46	6.71	9.18	3.01	4.20							
X(3)-S	2.65	4.22	6.64	8.53	3.17	4.80	7.08	9.06	7.39	9.41	0.38	2.40	0.0
X(3)-SDDMA	2.64	4.32	6.79	9.15	2.79	4.33	6.59	8.82	6.63	8.68	0.13	3.08	0.029
$^{190}\text{Pt}$ Expt.	2.49	4.35	6.47	8.57	3.11	4.07			(5.65)				
X(3)-S	2.69	4.17	6.50	8.24	3.01	4.50	6.72	8.52	6.93	8.72	0.25	2.96	0.0
X(3)-SDDMA	2.73	4.24	6.61	8.57	2.83	4.23	6.44	8.33	6.48	8.24	0.18	3.75	0.019
$^{192}\text{Pt}$ Expt.	2.48	4.31	6.38	8.62	3.78	4.55							
X(3)-S	2.65	4.23	6.66	8.57	3.19	4.84	7.13	9.14	7.45	9.50	0.30	2.34	0.0
X(3)-SDDMA	2.65	4.23	6.66	8.57	3.19	4.84	7.13	9.14	7.45	9.50	0.30	2.34	0.0
$^{194}\text{Pt}$ Expt.	2.47	4.30	6.39	8.67	3.23	4.60							
X(3)-S	2.64	4.24	6.69	8.63	3.86	4.91	7.20	9.25	7.55	9.65	0.19	2.25	0.0
X(3)-SDDMA	2.65	4.23	6.64	8.60	3.07	4.68	6.94	8.95	7.19	9.20	0.15	2.53	0.004
$^{196}\text{Pt}$ Expt.	2.47	4.29	6.33	8.56	3.19	3.83							
X(3)-S	2.72	4.15	6.45	8.13	2.96	4.39	6.59	8.31	6.76	8.46	0.33	3.25	0.0
X(3)-SDDMA	2.66	4.18	6.47	8.47	2.71	4.10	6.23	8.13	6.23	7.98	0.25	3.95	0.027
$^{146}\text{Nd}$ Expt.	2.30	3.92	5.72	7.32	2.02	2.87	3.85						
X(3)-S	2.34	3.56	5.14	6.46	2.32	3.45	4.96	6.26	4.96	6.19	0.64	5.88	0.0
X(3)-SDDMA	2.21	3.47	4.92	6.37	2.11	3.20	4.52	5.88	4.44	5.65	0.58	9.71	0.078
$^{148}\text{Nd}$ Expt.	2.49	4.24	6.15	8.19	3.04	3.88	5.32	7.12	(5.30)				
X(3)-S	2.61	3.95	5.98	7.49	2.71	3.98	5.94	7.46	6.02	7.48	0.39	4.15	0.0
X(3)-SDDMA	2.48	3.94	5.97	7.90	2.45	3.74	5.60	7.39	5.54	7.15	0.30	4.86	0.046
$^{150}\text{Sm}$ Expt.	2.32	3.83	5.50	7.29	2.22	3.13	4.34	6.31	(3.76)				
X(3)-S	2.36	3.60	5.23	6.57	2.36	3.51	5.06	6.39	5.07	6.33	0.41	5.58	0.0
X(3)-SDDMA	2.22	3.49	4.98	6.50	2.10	3.21	4.56	5.95	4.45	5.69	0.39	9.78	0.100
$^{152}\text{Sm}$ Expt.	3.01	5.80	9.24	13.21	5.62	6.65	8.40	10.76	8.89	10.62			
X(3)-S	2.55	4.43	7.14	9.55	4.10	6.20	8.55	11.19	9.36	12.20	1.59	1.16	0.0
X(3)-SDDMA	2.34	4.40	7.02	9.94	3.91	6.09	8.24	11.24	8.96	12.07	1.54	0.78	0.007
$^{154}\text{Gd}$ Expt.	3.01	5.83	9.30	13.3	5.53	6.63	8.51	11.10	9.60	11.52			
X(3)-S	2.53	4.46	7.21	9.70	4.33	6.50	8.84	11.58	9.75	12.74	1.51	0.99	0.0
X(3)-SDDMA	2.36	4.42	7.09	9.97	4.21	6.43	8.59	11.61	9.45	12.64	1.47	0.69	0.005
$^{156}\text{Dy}$ Expt.	2.93	5.59	8.82	12.52	4.90	6.01	7.90	10.43	10.00	11.52			
X(3)-S	2.53	4.46	7.20	9.68	4.31	6.46	8.81	11.53	9.71	12.68	1.28	1.01	0.0
X(3)-SDDMA	2.37	4.42	7.09	9.45	4.17	6.38	8.56	11.56	9.40	12.56	1.25	0.73	0.005

Another interesting aspect of the DDM effect that can be studied by the present model is whether or not a shape phase transition takes place within an isotopic chain.

For this reason, the fitted values of  $\varrho$  are plotted in Fig. 4 as a function of the neutron number  $N$  for the most isotopic chains considered in the present paper, namely,  $^{98-108}\text{Ru}$ ,  $^{146-150}\text{Nd}$ ,  $^{116-130}\text{Xe}$ , and  $^{180-196}\text{Pt}$ . Note that the continuous

lines indicate the shape evolution within the isotope chain, while the area between the dashed lines corresponds to the critical point region. Finally, the regions above and below the dashed lines correspond to the spherical and deformed regions, respectively.

For the isotopes of Ru, both the shape phase transition and the candidate for the critical point are totally sensitive

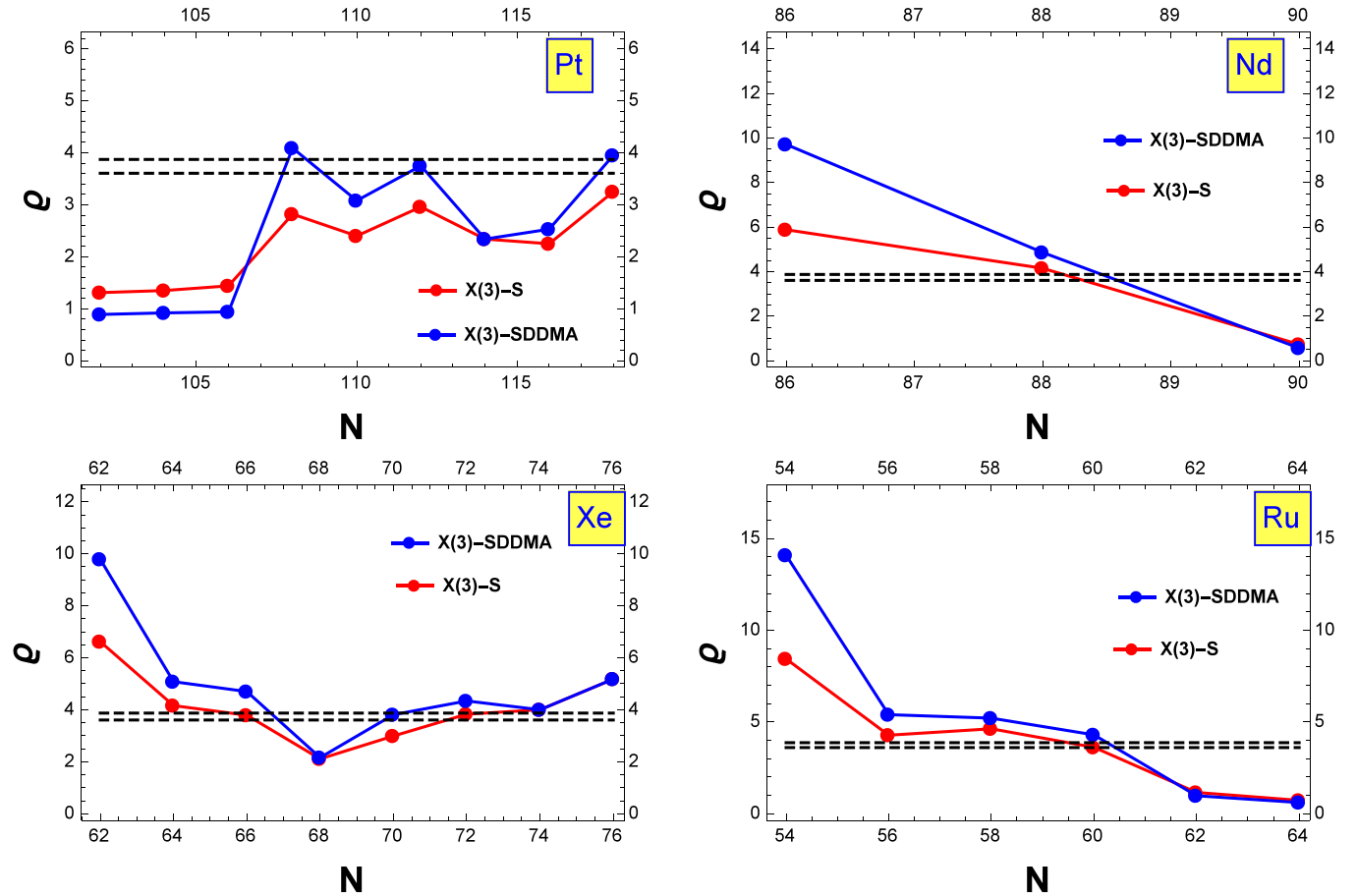


FIG. 4. Fitted values of the free parameter  $\rho$  for isotopes of Ru, Xe, Pt, and Nd are given as a function of the neutron number  $N$  where  $\tau = 0$  [21] (red lines) and  $\tau \neq 0$  (blue lines). Continuous lines indicate the shape evolution within the isotope chain, while the dashed ones are for the critical point region.

to the DDM parameter. Indeed, for the lighter nuclei, the DDM displaces the potential parameter  $\rho$  to large values with respect to the constant mass case ( $\tau = 0$ ). Then, the phase transition  $^{98}\text{Ru} \rightarrow ^{108}\text{Ru}$  occurs from the lightest isotope towards the heaviest one, which is similar to the sextic and ML approach [ $X(3)$ -SML] [73]. Indeed, in the case of ( $\tau \neq 0$ ), one has a crossing of the critical point by passing from  $^{104}\text{Ru}$  to  $^{106}\text{Ru}$ , while for ( $\tau = 0$ ) the  $^{104}\text{Ru}$  nucleus becomes the best candidate for the critical point of this transition. Moreover, the nuclei  $^{98}\text{Ru}$ ,  $^{100}\text{Ru}$ , and  $^{102}\text{Ru}$  tend to the more spherical region when  $\tau \neq 0$ .

A similar unidirectional shape phase transition was observed for the Nd isotopes ( $^{146}\text{Nd} \rightarrow ^{150}\text{Nd}$ ), where the dashed lines are crossed going from  $^{148}\text{Nd}$  to  $^{150}\text{Nd}$  in both cases ( $\tau = 0$  and  $\tau \neq 0$ ). Note that in the case of  $\tau \neq 0$  the lighter nucleus  $^{146}\text{Nd}$  is shifted to the more spherical shape.

The phase transition for the isotopes of Xe seems to be different from that of Ru, in which one has two intersections of the critical point: the first takes place from the lightest isotopes towards the medium ones ( $^{116}\text{Xe} \rightarrow ^{122}\text{Xe}$ ), while the second one is from the heaviest isotopes towards the medium ones ( $^{130}\text{Xe} \rightarrow ^{122}\text{Xe}$ ). In the DDM case ( $\tau \neq 0$ ), the lightest isotopes tend to large values of  $\rho$  with respect to the constant mass case ( $\tau = 0$ ).

Physically speaking, one can say that the phase transition takes place faster in the case of the constant mass than in the deformation-dependent one.

Important effects of the DDM were observed for the Pt isotopes, where the shape phase transition changes significantly compared to the description offered by the case where the mass is constant. In accordance with  $\tau \neq 0$ , the critical point region is crossed twice: once from  $^{186}\text{Pt}$  towards  $^{184}\text{Pt}$  and the second time from  $^{196}\text{Pt}$  to  $^{194}\text{Pt}$ , which is not the case when the mass parameter is constant. Indeed, for  $\tau = 0$ , there is no phase transition from a spherical shape to a deformed one. Also one can observe that for  $\tau \neq 0$  the lighter nuclei  $^{180-184}\text{Pt}$  are shifted to the more deformed region, while the heaviest ones  $^{186-196}\text{Pt}$  are shifted to the critical point region.

Other remarks can be drawn by analyzing Fig. 4; one can observe that the results concerning the shape of nuclei in the case of  $\tau \neq 0$  are totally different from those in  $\tau = 0$ . The best candidates for the critical point of the  $\gamma$ -rigid prolate harmonic vibrator to the  $\gamma$ -rigid anharmonic vibrator shape phase transition are found to be  $^{190,196}\text{Pt}$ ,  $^{124}\text{Xe}$ , and  $^{132}\text{Ce}$ . Other possible candidates can be also considered:  $^{186}\text{Pt}$ ,  $^{172}\text{Os}$ , and  $^{128}\text{Xe}$ . As can be seen in Ref. [34], the higher quasisixact solvability order changes dramatically the shape phase transition within an isotopic chain. Therefore, the combination of

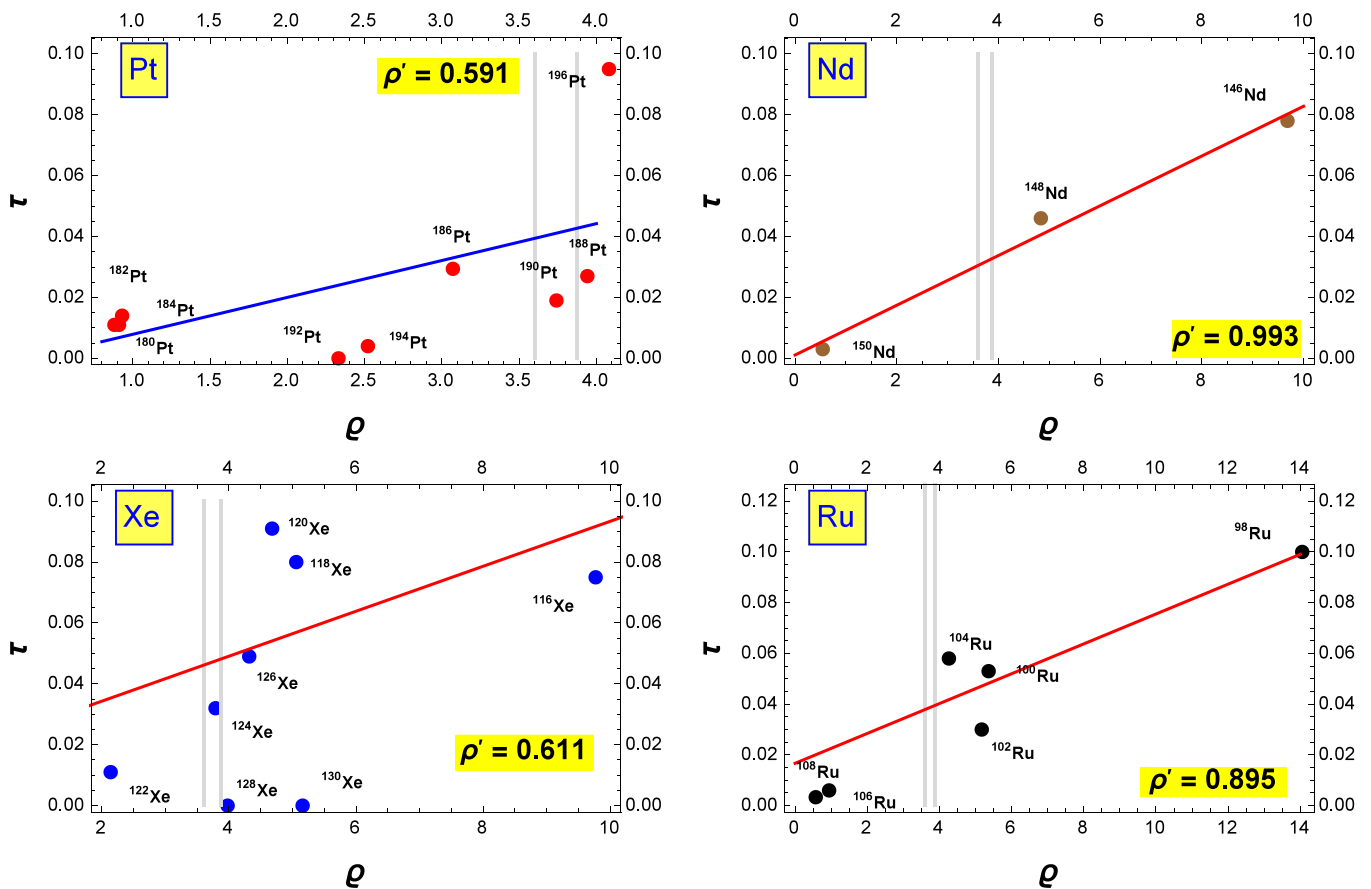


FIG. 5. Correlation between the potential parameter  $\rho$  and the DDM one  $\tau$  for isotopes of Ru, Xe, Pt, and Nd. Gray vertical lines indicate the critical point region.

the DDM in the higher order  $k > 2$  could offer, in this way, a more realistic description of these shape phase transitions, and it will be the topic of our future works.

The variations of the DDM parameter  $\tau$  as a function of  $\rho$  are shown in Fig. 5 for the most isotopic chains considered in this paper. By analyzing this figure, one can see that, excepting the nuclei  $^{128-130}\text{Xe}$  and  $^{192}\text{Pt}$  with the DDM parameter equal to zero, the DDM parameter  $\tau$  is spread between 0.003 and 0.1, between 0.003 and 0.1, between 0.011 and 0.091, and between 0.004 and 0.094 for Ru, Nd, Xe, and Pt isotopes, respectively. Thus, two different situations are presented here: the first one concerns the isotope chains with unidirectional shape phase transition, namely, Ru and Nd, where one can observe that the smallest value of  $\tau$  corresponds to the heaviest nuclei of each isotopes. The second case corresponds to the isotope chains with multidirectional shape phase transition, namely, Xe and Pt isotopes, where the smallest value of  $\tau$  corresponds to  $^{194}\text{Pt}$  and  $^{122}\text{Xe}$ , respectively. Another important remark that can be drawn from the analysis of these figures is the strong correlation observed between the potential parameter  $\rho$  and the DDM one  $\tau$  for the isotope chains of Ru and Nd, where the cross-correlation coefficient  $\rho'$  is greater than 90% in both cases of Ru and Nd isotopes. Such a correlation for the Xe and Pt isotopes becomes 61 and 59%, respectively. Then one can conclude that this correlation is more pronounced for

the isotope chains the shape phase transitions of which are unidirectional.

### C. $B(E2)$ transition rates

Before dealing with the  $B(E2)$  transition rates, it is necessary to determine  $\tau_{\text{lim}}$ : the value which shows the limitation of the perturbation term for the present model. Basically, it is made by analyzing the wave functions as well as the corresponding density probability distribution.

Thus, in Fig. 6 the behaviors of the wave functions are plotted versus  $y$  for the special value of the potential parameter  $\rho = 3$  and  $\tau$  values varying from 0 to 1.

By analyzing these data, the following remarks deserve to be made: Below  $\tau = 0.15$ , the wave functions of the ground state  $\eta_{0,0}^{\text{corr}}$  and the first excited state  $\eta_{1,0}^{\text{corr}}$  maintain the same shape as those related to the constant mass case ( $\tau = 0$ ) and of the  $X(3)$  model [31]. The additional effect consists in a slight shift towards the higher values of  $y$ . However, for  $\tau > 0.15$ , additional nodes are observed for both wave functions  $\eta_{0,0}^{\text{corr}}$  and  $\eta_{1,0}^{\text{corr}}$ .

Therefore, the limit of perturbations for this paper is  $\tau_{\text{lim}} = 0.15$ . This is taken into account in the numerical results. Indeed, according to Tables I and II, the maximum fitted value of  $\tau$  is 0.1.

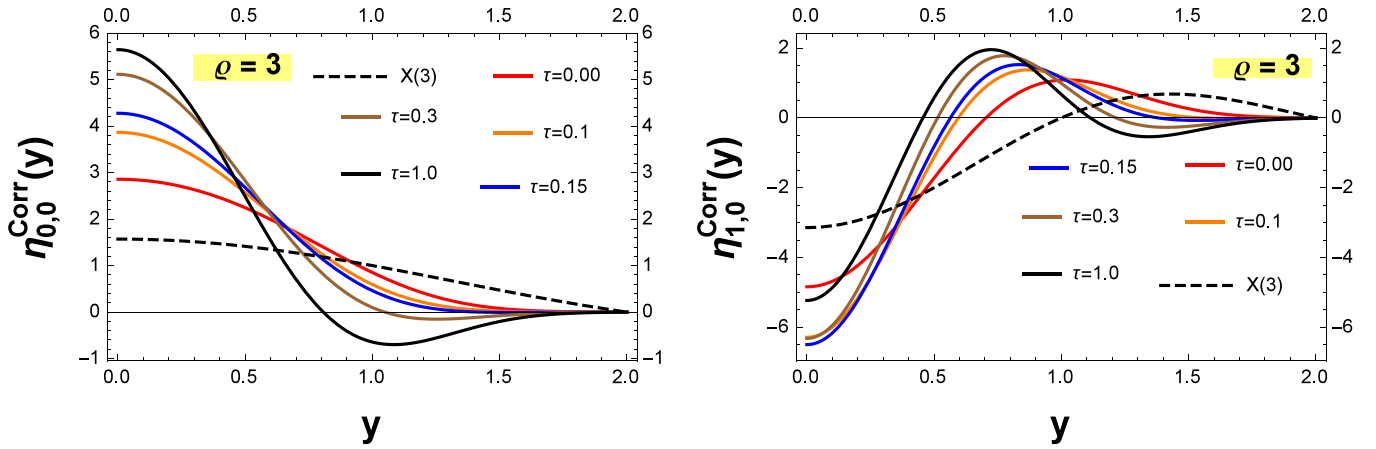


FIG. 6. Corrected wave function drawn as a function of  $y$  and free parameters  $\rho$  and  $\tau$  for the ground state labeled by  $\eta_{0,0}^{\text{Corr}}$  and for the first excited  $\beta$  state labeled by  $\eta_{1,0}^{\text{Corr}}$  for the case  $\rho = 3$  and varying  $\tau$  from 0 to 1.

The same remark holds for the density probability distribution, which is plotted in Fig. 7 as a function of  $y$ . Indeed, beyond the limit  $\tau = 0.15$ , the density probability plots show supplementary peaks, which means that we are getting away from the ground state  $\rho_{0,0}^{\text{Corr}}$  and from the first excited  $\beta$  state  $\rho_{1,0}^{\text{Corr}}$  corresponding to the constant mass case ( $\tau = 0$ ). Additionally, these peaks rise slowly with the DDM parameter  $\tau$ .

Other important observables for quadrupole collective states are the electromagnetic  $E2$  transition probabilities. Several  $B(E2)$  ratios normalized to the transition from the first excited state to the ground state g.s. band are presented in Tables III and IV and calculated with our model for 35 nuclei. Taking into account the fact that the two free parameters  $\rho$  and  $\tau$  were fitted only for the energy spectra and listed in Tables I and II, one can see that the results are generally in agreement with the experimental data, in particular for the nuclei  $^{150}\text{Nd}$ ,  $^{154}\text{Gd}$ , and  $^{156}\text{Dy}$ , which are known from the literature as good candidates for  $X(5)$ . Moreover, we can also see that the DDM improves the  $8_1 \rightarrow 6_1$  transition. Finally, for some nuclei, whether for the constant mass case or for the DDM

one, the transition probabilities seem to be overestimated. One can improve the agreement with experimental data by using alternatively a harmonic and an anharmonic transition operator for the calculation of  $E2$  transition probabilities as was made in Ref. [74].

#### D. Correlation between the minimal length formalism and the DDM in the frame of the $X(3)$ -sextic

In this subsection we will deal with the correlation between the ML [73] and the DDM, which are two quantum concepts widely used in different fields of physics. This correlation was observed for the first time in Ref. [75], where it was revealed in transitional nuclei near the CPSs  $X(3)$  and  $Z(4)$  within Infinite Square Well and Davidson potentials through calculations of their energy spectra, moments of inertia, and transition probabilities.

This correlation has been used as a new signature for some nuclear CPSs. In the present paper we check if this correlation between the DDM and ML parameters persists for the case of the sextic potential near the  $X(3)$  CPS. First, we recall that the ML formalism or generalized uncertainty principle

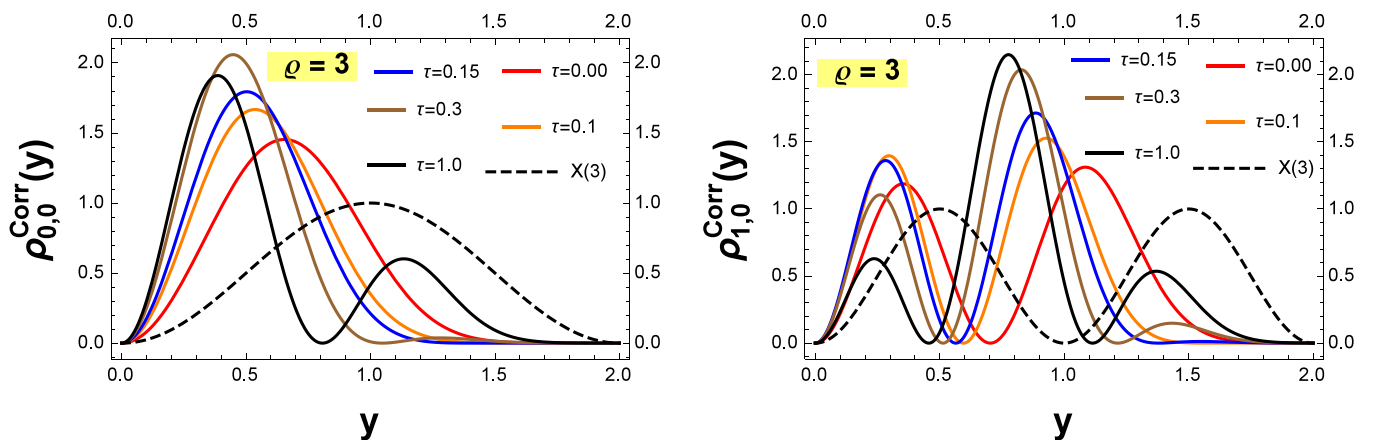


FIG. 7. Density of probability distribution drawn as a function of  $y$  and free parameters  $\rho$  and  $\tau$  for the ground state labeled by  $\rho_{0,0}^{\text{Corr}}$  and for the first excited  $\beta$  state labeled by  $\rho_{1,0}^{\text{Corr}}$  for the case  $\rho = 3$  and varying  $\tau$  from 0 to 1.

TABLE III. Several  $B(E2)$  transition rates normalized as in Eq. (58) are compared with the available experimental data [43–47,50–57,67–69] and with results available in Ref. [21] of the nuclei  $^{98-108}\text{Ru}$ ,  $^{100-102}\text{Mo}$ ,  $^{132-134}\text{Ce}$ ,  $^{150-152}\text{Sm}$ ,  $^{146-150}\text{Nd}$ ,  $^{154}\text{Gd}$ ,  $^{156}\text{Dy}$ , and  $^{172}\text{Os}$ . In the first line of each nucleus are given the experimental data, in the second line are the corresponding  $X(3)\text{-S}$  [21], while in third line are the corresponding theoretical results with ( $\lambda = \delta = 0$ ).

Nucleus	$\frac{4_1 \rightarrow 2_1}{2_1 \rightarrow 0_1}$	$\frac{6_1 \rightarrow 4_1}{2_1 \rightarrow 0_1}$	$\frac{8_1 \rightarrow 6_1}{2_1 \rightarrow 0_1}$	$\frac{10_1 \rightarrow 8_1}{2_1 \rightarrow 0_1}$	$\frac{0_\beta \rightarrow 2_1}{2_1 \rightarrow 0_1}$	$\frac{2_\beta \rightarrow 2_1}{2_1 \rightarrow 0_1}$	$\frac{2_\beta \rightarrow 4_1}{2_1 \rightarrow 0_1}$	$\frac{2_\beta \rightarrow 0_\beta}{2_1 \rightarrow 0_1}$
$^{98}\text{Ru}$ Expt.	0.38(11)	0.40(8)	0.08(2)					
$X(3)\text{-S}$	2.34	3.48	4.62	5.62	3.21	0.21	1.47	1.52
$X(3)\text{-SDDMA}$	2.36	3.56	4.71	6.02	3.26	0.22	1.57	1.60
$^{100}\text{Ru}$ Expt.	1.43(11)	4.78(5)			0.98(14)			
$X(3)\text{-S}$	2.23	3.08	3.98	4.63	2.83	0.18	1.02	1.24
$X(3)\text{-SDDMA}$	2.24	3.14	3.93	5.27	2.88	0.20	1.10	1.33
$^{102}\text{Ru}$ Expt.	1.48(25)	1.52(56)	1.26(43)	1.28(47)	0.78(14)			
$X(3)\text{-S}$	2.25	3.15	4.08	4.77	2.90	0.19	1.09	1.28
$X(3)\text{-SDDMA}$	2.25	3.16	4.03	5.12	2.90	0.20	1.11	1.32
$^{104}\text{Ru}$ Expt.	1.43(16)			0.43(5)				
$X(3)\text{-S}$	2.18	2.94	3.76	4.31	2.65	0.17	0.88	1.15
$X(3)\text{-SDDMA}$	2.16	2.93	3.50	5.06	2.63	0.19	0.90	1.21
$^{106}\text{Ru}$ Expt.								
$X(3)\text{-S}$	1.75	2.07	2.47	2.67	1.22	0.09	0.24	0.69
$X(3)\text{-SDDMA}$	1.72	2.02	2.42	2.75	1.14	0.09	0.22	0.67
$^{108}\text{Ru}$ Expt.	1.65(20)							
$X(3)\text{-S}$	1.66	1.93	2.27	2.43	0.95	0.08	0.16	0.64
$X(3)\text{-SDDMA}$	1.64	1.90	2.25	2.47	0.90	0.077	0.15	0.63
$^{100}\text{Mo}$ Expt.	1.86(11)	2.54(38)	3.32(49)		2.49(12)	$\approx 0$	0.97(49)	0.38(11)
$X(3)\text{-S}$	2.35	3.49	4.64	5.64	3.21	0.21	1.48	1.53
$X(3)\text{-SDDMA}$	2.34	3.47	4.54	5.88	3.19	0.22	1.47	1.55
$^{102}\text{Mo}$ Expt.	1.20(28)			0.95(42)				
$X(3)\text{-S}$	2.05	2.64	3.31	3.71	2.23	0.15	0.62	0.97
$X(3)\text{-SDDMA}$	2.11	2.83	3.10	5.24	2.48	0.18	0.83	1.18
$^{132}\text{Ce}$ Expt.	0.75(17)	0.27(10)	0.47(4)	0.07(2)				
$X(3)\text{-S}$	2.00	2.53	3.15	3.51	2.06	0.14	0.54	0.91
$X(3)\text{-SDDMA}$	2.09	2.77	3.12	4.97	2.41	0.18	0.77	1.12
$^{134}\text{Ce}$ Expt.	0.75(17)	0.27(10)	0.47(4)	0.07(2)				
$X(3)\text{-S}$	1.91	2.35	2.88	3.17	1.75	0.12	0.41	0.82
$X(3)\text{-SDDMA}$	1.90	2.34	2.87	3.23	1.73	0.12	0.41	0.82
$^{150}\text{Sm}$ Expt.	1.93(30)	2.63(88)	2.98(158)		0.93(9)			$1.93^{+0.70}_{-0.53}$
$X(3)\text{-S}$	2.29	3.28	4.30	5.09	3.03	0.20	1.23	1.37
$X(3)\text{-SDDMA}$	2.33	3.44	4.46	5.86	3.17	0.22	1.43	1.53
$^{152}\text{Sm}$ Expt.	1.44(2)	1.66(3)	2.02(4)	$2.17^{+0.24}_{-0.18}$	0.23(1)	0.04	0.12(1)	1.17(8)
$X(3)\text{-S}$	1.66	1.94	2.30	2.65	0.98	0.09	0.18	0.61
$X(3)\text{-SDDMA}$	1.68	1.96	2.33	2.68	1.03	0.09	0.19	0.65
$^{146}\text{Nd}$ Expt.	1.47(39)							
$X(3)\text{-S}$	2.30	3.31	4.35	5.17	3.06	0.20	1.27	1.40
$X(3)\text{-SDDMA}$	2.34	3.46	4.51	5.83	3.18	0.22	1.45	1.53
$^{148}\text{Nd}$ Expt.	1.62(9)	1.76(14)	1.69(30)		0.54(4)	0.25(3)	0.28(14)	
$X(3)\text{-S}$	2.22	3.06	3.94	4.57	2.80	0.18	1.00	1.23
$X(3)\text{-SDDMA}$	2.22	3.07	3.82	5.11	2.80	0.20	1.03	1.28
$^{150}\text{Nd}$ Expt.	1.56(4)	1.78(9)	1.86(20)	1.73(10)	0.37(2)	0.09(3)	0.16(6)	1.38(112)
$X(3)\text{-S}$	1.66	1.93	2.27	2.43	0.95	0.08	0.16	0.64
$X(3)\text{-SDDMA}$	1.64	1.89	2.22	2.42	0.87	0.07	0.14	0.62
$^{154}\text{Gd}$ Expt.	1.56(6)	1.82(10)	1.99(11)	2.29(26)	0.33(5)	0.04	0.12(1)	0.62(6)
$X(3)\text{-S}$	1.71	2.01	2.39	2.57	1.11	0.09	0.20	0.67
$X(3)\text{-SDDMA}$	1.66	1.93	2.28	2.56	0.96	0.08	0.17	0.63
$^{156}\text{Dy}$ Expt.	1.63(2)	1.87(6)	2.07(20)	2.20(27)		0.09(3)	0.08(3)	
$X(3)\text{-S}$	1.66	1.92	2.8	2.56	0.94	0.08	0.17	0.61
$X(3)\text{-SDDMA}$	1.67	1.94	2.30	2.58	0.98	0.08	0.18	0.63
$^{172}\text{Os}$ Expt.	1.50(17)	2.61(38)	3.30(98)	1.65(36)				
$X(3)\text{-S}$	2.21	3.03	3.90	4.51	2.76	0.18	0.97	1.21
$X(3)\text{-SDDMA}$	2.22	3.08	3.88	5.07	2.82	0.20	1.04	1.28

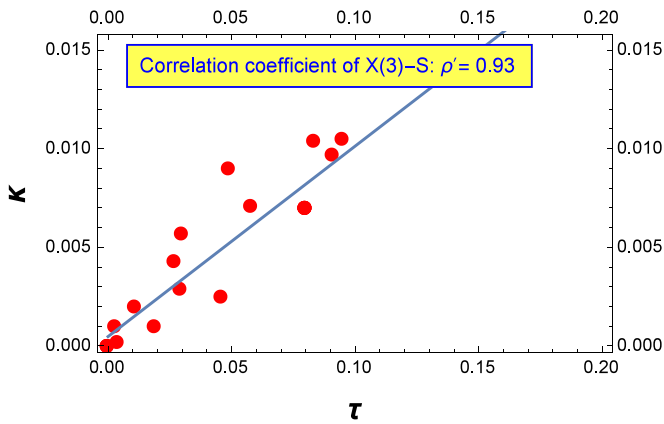
TABLE IV. Same as in Table III, but for the available experimental data [48,49,58–66,69–72] of the nuclei  $^{118-130}\text{Xe}$  and  $^{180-196}\text{Pt}$ .

Nucleus	$\frac{4_1 \rightarrow 2_1}{2_1 \rightarrow 0_1}$	$\frac{6_1 \rightarrow 4_1}{2_1 \rightarrow 0_1}$	$\frac{8_1 \rightarrow 6_1}{2_1 \rightarrow 0_1}$	$\frac{10_1 \rightarrow 8_1}{2_1 \rightarrow 0_1}$	$\frac{0_\beta \rightarrow 2_1}{2_1 \rightarrow 0_1}$	$\frac{2_\beta \rightarrow 2_1}{2_1 \rightarrow 0_1}$	$\frac{2_\beta \rightarrow 4_1}{2_1 \rightarrow 0_1}$	$\frac{2_\beta \rightarrow 0_\beta}{2_1 \rightarrow 0_1}$
$^{118}\text{Xe}$ Expt.	1.11(6)	0.88(23)	0.49(18)	>0.7				
$X(3)$ -S	2.22	3.06	3.95	4.58	2.80	0.18	1.00	1.23
$X(3)$ -SDDMA	2.20	3.02	3.60	5.35	2.74	0.20	0.99	1.28
$^{120}\text{Xe}$ Expt.	1.16(10)	1.17(19)	0.96(17)	0.91(16)				
$X(3)$ -S	2.19	2.98	3.82	4.40	2.70	0.18	0.91	1.17
$X(3)$ -SDDMA	2.15	2.93	3.32	5.37	2.62	0.19	0.91	1.24
$^{122}\text{Xe}$ Expt.	1.46(11)	1.41(9)	1.03(8)	1.54(10)				
$X(3)$ -S	1.95	2.44	3.01	3.33	1.90	0.13	0.47	0.86
$X(3)$ -SDDMA	1.95	2.45	3.01	3.58	1.92	0.14	0.49	0.88
$^{124}\text{Xe}$ Expt.	1.17(4)	1.52(14)	1.14(36)	0.36(5)				
$X(3)$ -S	2.10	2.76	3.48	3.94	2.40	0.16	0.72	1.04
$X(3)$ -SDDMA	2.15	2.89	3.58	4.70	2.59	0.18	0.86	1.16
$^{126}\text{Xe}$ Expt.								
$X(3)$ -S	2.20	2.99	3.83	4.42	2.71	0.18	0.93	1.18
$X(3)$ -SDDMA	2.18	2.96	3.62	5.00	2.67	0.19	0.93	1.22
$^{128}\text{Xe}$ Expt.	1.47(15)	1.94(20)	2.39(30)					
$X(3)$ -S	2.21	3.03	3.89	4.50	2.76	0.18	0.97	1.20
$X(3)$ -SDDMA	2.21	3.03	3.89	4.50	2.76	0.18	0.97	1.20
$^{130}\text{Xe}$ Expt.								
$X(3)$ -S	2.28	3.23	4.22	4.97	2.99	0.19	1.18	1.34
$X(3)$ -SDDMA	2.28	3.23	4.22	4.97	2.99	0.19	1.18	1.34
$^{180}\text{Pt}$ Expt.	0.92(22)	$\geq 0.29$						
$X(3)$ -S	1.78	2.12	2.55	2.77	1.33	0.10	0.27	0.72
$X(3)$ -SDDMA	1.70	2.00	2.37	2.85	1.12	0.10	0.22	0.65
$^{182}\text{Pt}$ Expt.								
$X(3)$ -S	1.79	2.14	2.57	2.80	1.36	0.10	0.28	0.72
$X(3)$ -SDDMA	1.71	2.01	2.38	2.89	1.14	0.10	0.22	0.66
$^{184}\text{Pt}$ Expt.	1.65(9)	1.78(12)	2.13(16)	2.44(33)				
$X(3)$ -S	1.81	2.17	2.62	2.86	1.42	0.10	0.30	0.74
$X(3)$ -SDDMA	1.72	2.02	2.37	2.98	1.18	0.1	0.23	0.66
$^{186}\text{Pt}$ Expt.								
$X(3)$ -S	2.08	2.70	3.40	3.83	2.32	0.15	0.67	1.01
$X(3)$ -SDDMA	2.10	2.81	2.95	5.35	2.45	0.18	0.81	1.17
$^{188}\text{Pt}$ Expt.								
$X(3)$ -S	2.01	2.55	3.17	3.54	2.08	0.14	0.55	0.92
$X(3)$ -SDDMA	2.07	2.71	3.29	4.38	2.34	0.17	0.70	1.05
$^{190}\text{Pt}$ Expt.								
$X(3)$ -S	2.10	2.75	3.46	3.92	2.39	0.16	0.71	1.03
$X(3)$ -SDDMA	2.16	2.91	3.68	4.55	2.62	0.18	0.87	1.15
$^{192}\text{Pt}$ Expt.	1.56(9)	1.22(53)						
$X(3)$ -S	2.00	2.53	3.14	3.50	2.05	0.14	0.54	0.91
$X(3)$ -SDDMA	2.00	2.53	3.14	3.50	2.05	0.14	0.54	0.91
$^{194}\text{Pt}$ Expt.	1.73(11)	1.36(43)	1.02(29)	0.69(18)				
$X(3)$ -S	1.98	2.49	3.09	3.43	1.99	0.14	0.51	0.89
$X(3)$ -SDDMA	2.03	2.59	3.23	3.69	2.15	0.15	0.59	0.95
$^{196}\text{Pt}$ Expt.	1.48(2)	1.80(10)	1.92(25)				$\approx 0$	0.12(12)
$X(3)$ -S	2.14	2.83	3.60	4.10	2.51	0.17	0.79	1.09
$X(3)$ -SDDMA	2.16	2.92	3.62	4.74	2.63	0.18	0.89	1.18

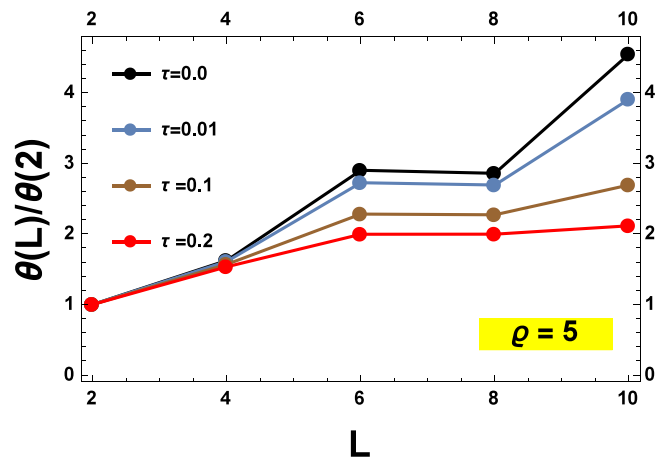
corresponds to deformed commutation relations. The solutions of the Bohr Hamiltonian in the presence of ML are derived by means of QES and QPM in Ref. [73], where the obtained energy spectra normalized to the energy of the first excited state for the ground state band are given as a function of two parameters, namely, the sextic potential parameter  $\varrho$  and the ML one  $\kappa$ .

Now, dealing with concrete nuclei, the energy ratios (61) are calculated for different levels of the g.s. and two  $\beta$  bands for  $X(3)$ -SML [73] and the present model  $X(3)$ -SDDMA. The 16 even-even nuclei used for the  $X(3)$ -SML and  $X(3)$ -SDDMA models belong to the following isotope chains:  $^{118-122}\text{Xe}$ ,  $^{126-130}\text{Xe}$ ,  $^{102}\text{Mo}$ ,  $^{102,104}\text{Ru}$ ,  $^{148}\text{Nd}$ ,  $^{134}\text{Ce}$ , and  $^{188,196}\text{Pt}$ . We have chosen the nuclei for which the ratio  $R_{0,4}$  is

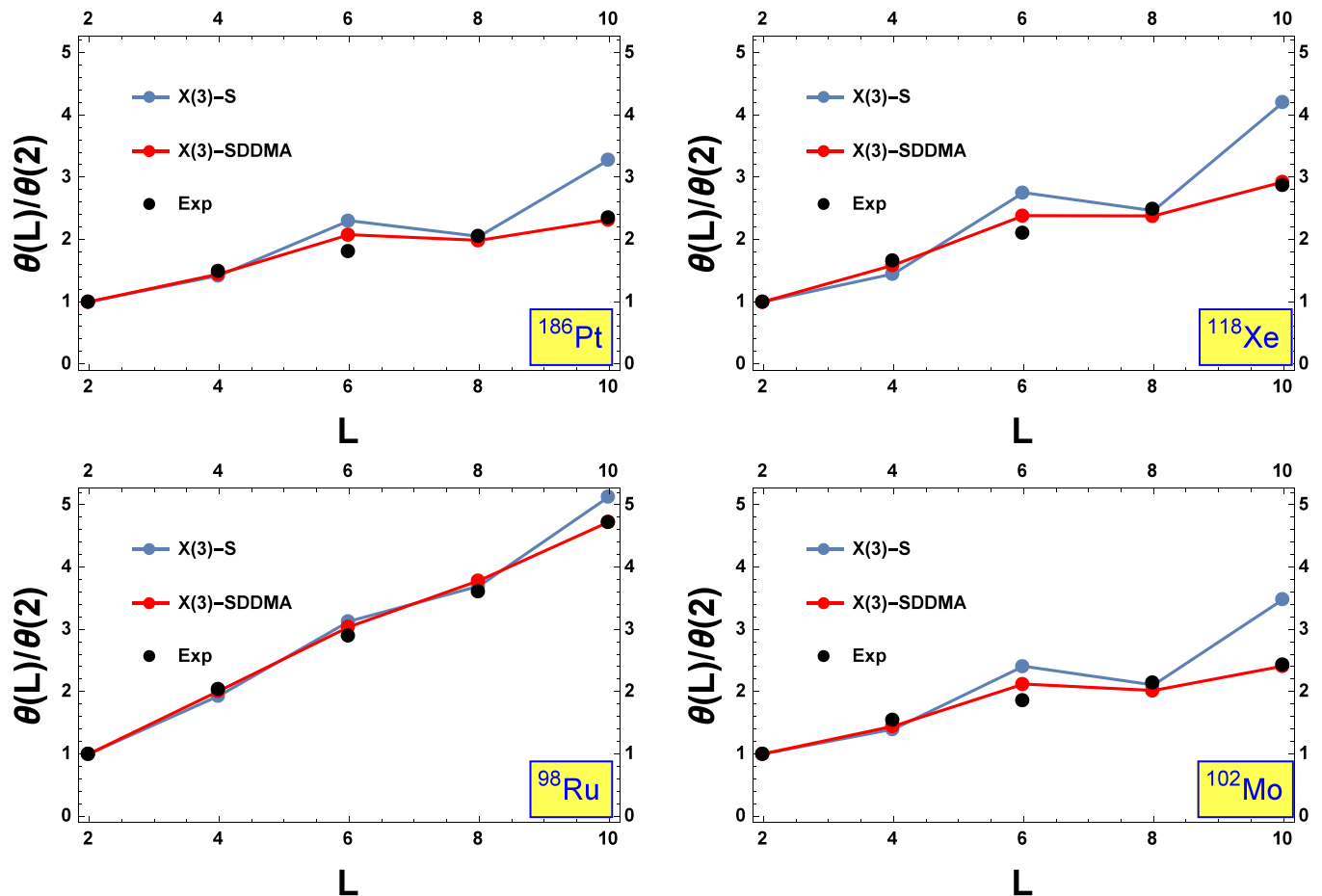


FIG. 8. Correlation between the ML parameter  $\kappa$  and DDM one  $\tau$ .

not far from the value 2.44, which is a reference point for the  $X(3)$  model. The obtained values for the parameters  $\kappa$  [73] and  $\tau$  from the fit on all available experimental data are depicted in Fig. 8. Indeed, this figure shows a strong correlation between ML and DDM concepts where the cross-correlation coefficient is greater than 90%. As a result, this correlation persists for the sextic potential case with the QES order  $k = 2$ . Also, by comparing the present model with  $X(3)$ -SML [73],

FIG. 9. Moment of inertia for the g.s. band, given by Eq. (63) normalized to the moment of the  $2^+$  state plotted as a function of  $L$  are shown for the specific value of  $\varrho = 5$ , and varying DDM parameter  $\tau$ .

one can see that the difference between the obtained theoretical results in their framework is not significant. Such a fact is clearly related to the existent correlation between the two concepts.

FIG. 10. Moment of inertia for the g.s. band normalized to the moment of the  $2^+$  state plotted as a function of  $L$  compared with the available experimental data [50,52,62,70] of the nuclei  $^{98}\text{Ru}$ ,  $^{102}\text{Mo}$ ,  $^{118}\text{Xe}$ , and  $^{186}\text{Pt}$ .

### E. DDM effect on the moment of inertia of the ground state

The moment of inertia is a physical quantity which describes the kinematics of nuclei in rotational motion mode. Classically, it is defined as the ratio of the angular momentum  $L$  to the angular velocity  $\omega$  which is not an observable. In this last subsection, we are dealing with the DDM effect on the variation of this quantity. That is why we analyze the plot of the moment of inertia  $\theta(L)$  as a function of angular momentum  $L$ .

In practice, for the moment of inertia, we often use the relation given by Ref. [76]:

$$\theta(L) = \frac{R}{\omega} = \frac{1}{2} \frac{dE}{dR^2} \approx \frac{2L-1}{E(L)-E(L-2)}, \quad R^2 = L(L+1). \quad (63)$$

In Fig. 9, we plot the moment of inertia for the g.s. band normalized to the moment of the  $2^+$  state given by Eq. (63) as a function of  $L$  for the specific value of  $\varrho = 5$  and varying DDM parameter  $\tau$ . By carefully analyzing this figure, one can see that the remarkable increase of the moment of inertia with  $L$  observed where the mass is constant ( $\tau = 0$ ) is gradually moderated by increasing the DDM parameter  $\tau$ . We recall that this result has been proved for the first time in Ref. [13] and later on in Refs. [14,17].

For the application with experimental data, a plot of the normalized moment of inertia as a function of the total angular momentum  $L$  is given in Fig. 10 for the following isotopes:  $^{98}\text{Ru}$ ,  $^{102}\text{Mo}$ ,  $^{118}\text{Xe}$ , and  $^{186}\text{Pt}$ . From this figure, one can see that the corresponding experimental moment of inertia to these nuclei are well reproduced within the DDM concept with respect to the sextic potential in the constant mass case [21]. Before going to conclusions, it is important to pinpoint some drawbacks of the present model. The notable one is the impossibility to describe the  $\gamma$  band. Indeed, the present approach only describes the experimental data of the g.s. and first two  $\beta$  bands. However, the  $\gamma$  band is well described for the  $\gamma$ -rigid mode with the rigidity  $\gamma = \pi/6$  using the anharmonic sextic potential. This is made by the Davydov-Chaban Hamiltonian [22], where the mass parameter was considered as a constant. Nevertheless, the present solution can be useful in the understanding of the critical point phenomena. The application of the deformation-dependent effective mass to the Davydov-Chaban Hamiltonian with the sextic potential could improve the numerical realization with respect to  $Z(4)$ -sextic type solutions [22], and it will be the topic of our future work.

### IV. CONCLUSION

Here we shall summarize the main results presented in the present paper. We have solved the eigenvalues problem with the Bohr collective Hamiltonian for  $\gamma$ -rigid nuclei within a model by combining two model approaches: the quantum mechanical formalism, namely, DDM, and the anharmonic sextic oscillator potential for the variable  $\beta$  and  $\gamma = 0$ . The model is conventionally called  $X(3)$ -SDDMA. The Hamiltonian of the system has been conjointly solved by means of QES and a QPM. Thanks to the choice of the deformation function, the model was constructed in such a way that the scaling property was maintained as in Ref. [21]. Finally, the energy spectrum and the wave functions are given in analytical form. These depend on two free parameters  $\varrho$  and  $\tau$ . Numerical applications are done for 35 nuclei:  $^{98-108}\text{Ru}$ ,  $^{100-102}\text{Mo}$ ,  $^{116-130}\text{Xe}$ ,  $^{180-196}\text{Pt}$ ,  $^{172}\text{Os}$ ,  $^{146-150}\text{Nd}$ ,  $^{132-134}\text{Ce}$ ,  $^{154}\text{Gd}$ ,  $^{156}\text{Dy}$ , and  $^{150-152}\text{Sm}$ . The results are compared with the corresponding experimental data as well as with those obtained through  $X(3)$ -sextic, where the mass parameter was considered to be a constant [21]. The comparison of the rms values yielded by the DDM formalism produces the best agreement with the experimental energies. Concerning the  $B(E2)$  transitions, one can say that the corresponding theoretical results are slightly improved. Additionally, the DDM removed partially the approximate degeneracy of states with different angular momenta  $\Delta L = 2$  belonging to different bands observed in the critical point. The shape phase transition within an isotopic chain is changed in the DDM case compared to the case when the mass is considered as constant, where the new candidates for the critical point of the shape phase transition from a  $\gamma$ -rigid prolate harmonic vibrator to an anharmonic one are found to be  $^{190,196}\text{Pt}$ ,  $^{124}\text{Xe}$ , and  $^{132}\text{Ce}$ . The comparison between the two quantum concepts of the ML and DDM confirmed that they are well and truly correlated. Moreover, the dependence of the mass on the deformation moderates the increase of the moment of inertia with the deformation, removing an important drawback of the model  $X(3)$ -sextic [21] and leading to an overall agreement with the experimental data, results which are in concordance with those of Refs. [13,14,17]. The results obtained in the present paper open a door toward new future application such as considering the quasisexact solvability orders  $k > 2$  for  $X(3)$ -SDDMA and verifying if the theoretical results will be improved more than in the case of  $k = 2$ .

[1] A. Bohr, Dan. Vidensk. Selsk **26**, 1 (1952).  
 [2] A. Bohr and B. R. Mottelson, K. Dan. Vidensk. Selsk. Mat. Fys. Medd **27**, 16 (1953).  
 [3] P. Cejnar, J. Jolie, and R. F. Casten, *Rev. Mod. Phys.* **82**, 2155 (2010).  
 [4] F. Iachello, *Phys. Rev. Lett.* **85**, 3580 (2000).  
 [5] F. Iachello, *Phys. Rev. Lett.* **87**, 052502 (2001).  
 [6] F. Iachello, *Phys. Rev. Lett.* **91**, 132502 (2003).  
 [7] D. Bonatsos, D. Lenis, D. Petrellis, and P. A. Terziev, *Phys. Lett. B* **588**, 172 (2004).

[8] G. H. Wannier, *Phys. Rev.* **52**, 191 (1937).  
 [9] J. C. Slater, *Phys. Rev.* **76**, 1592 (1949).  
 [10] J. M. Slater and W. Kohn, *Phys. Rev.* **97**, 869 (1995).  
 [11] G. Bastard, *Wave Mechanics Applied to Semiconductor Heterostructures* (Editions de Physique, Les Ulis, 1988).  
 [12] L. Serra and E. Lipparini, *Europhys. Lett.* **40**, 667 (1997).  
 [13] D. Bonatsos, P. Georgoudis, D. Lenis, N. Minkov, and C. Quesne, *Phys. Lett. B* **683**, 264 (2010).  
 [14] D. Bonatsos, P. E. Georgoudis, D. Lenis, N. Minkov, and C. Quesne, *Phys. Rev. C* **83**, 044321 (2011).

- [15] C. Quesne and V. Tkachuk, *J. Phys. A: Math. Gen.* **37**, 4267 (2004).
- [16] M. Chabab, A. Lahbas, and M. Oulne, *Phys. Rev. C* **91**, 064307 (2015).
- [17] D. Bonatsos, P. E. Georgoudis, N. Minkov, D. Petrellis, and C. Quesne, *Phys. Rev. C* **88**, 034316 (2013).
- [18] P. Baganu, M. Chabab, A. El Batoul, A. Lahbas, and M. Oulne, *Nucl. Phys. A* **970**, 272 (2018).
- [19] A. G. Ushveridze, *Quasi-Exactly Solvable Models in Quantum Mechanics* (Institute of Physics, University of Reading, Berkshire, 1994).
- [20] F. Brau, *J. Phys. A: Math. Gen.* **32**, 7691 (1999).
- [21] P. Baganu and R. Budaca, *J. Phys. G: Nucl. Part. Phys.* **42**, 105106 (2015).
- [22] R. Budaca, P. Baganu, M. Chabab, A. Lahbas, and M. Oulne, *Ann. Phys. (NY)* **375**, 65 (2016).
- [23] G. Levai and J. M. Arias, *Phys. Rev. C* **69**, 014304 (2004).
- [24] G. Levai and J. M. Arias, *Phys. Rev. C* **81**, 044304 (2010).
- [25] T. Barakat, *Phys. Lett. A* **344**, 411 (2005).
- [26] R. L. Somorjai and D. F. Hornig, *J. Chem. Phys.* **36**, 1980 (1962).
- [27] C. Quigg and J. L. Rosner, *Phys. Rep.* **56**, 167 (1979).
- [28] P. Baganu and R. Budaca, *Phys. Rev. C* **91**, 014306 (2015).
- [29] R. Budaca, A. I. Budaca, and P. Baganu, *J. Phys. G: Nucl. Part. Phys.* **46**, 125102 (2019).
- [30] O. von Roos, *Phys. Rev. B* **27**, 7547 (1983).
- [31] D. Bonatsos, D. Lenis, D. Petrellis, P. Terziev, and I. Yigitoglu, *Phys. Lett. B* **632**, 238 (2006).
- [32] A. G. Sitenko and V. k. Tartakovskii, *Lectures on the Theory of the Nucleus* (Atomizdat, Moscow, 1972).
- [33] J. M. Eisenberg and W. Greiner, *Nuclear Theory, Nuclear Models* (North-Holland, Amsterdam, 1970), Vol. 1.
- [34] M. Oulne and I. Tagdamte, *J. Phys. G: Nucl. Part. Phys.* **49**, 035102 (2022).
- [35] M. Chabab, A. El Batoul, A. Lahbas, and M. Oulne, *Ann. Phys. (NY)* **392**, 142 (2018).
- [36] A. P. Prudnikov, Yu. A. Brychkov, and O. I. Marichev, *Integrals and Series* (Gordon and Breach, New York, 1986), Vol. 1.
- [37] M. Abramowitz and I. A. Stegun, *Handbook of Mathematical Functions* (Dover, New York, 1970).
- [38] A. Arima and F. Iachello, *Ann. Phys. (NY)* **99**, 253 (1976).
- [39] D. J. BenDaniel and C. B. Duke, *Phys. Rev.* **152**, 683 (1966).
- [40] M. Chabab, A. El Batoul, A. Lahbas, and M. Oulne, *J. Phys. G: Nucl. Part. Phys.* **43**, 125107 (2016).
- [41] D. Bonatsos, N. Minkov, and D. Petrellis, *J. Phys. G* **42**, 095104 (2015).
- [42] R. Budaca, *Eur. Phys. J. A* **50**, 87 (2014).
- [43] J. Blachot, *Nucl. Data Sheets* **111**, 717 (2010).
- [44] K. Kitao, *Nucl. Data Sheets* **75**, 99 (1995).
- [45] K. Kitao, Y. Tendow, and A. Hashizume, *Nucl. Data Sheets* **96**, 241 (2002).
- [46] T. Tamura, *Nucl. Data Sheets* **108**, 455 (2007).
- [47] J. Katakura and Z. D. Wu, *Nucl. Data Sheets* **109**, 1655 (2008).
- [48] J. Katakura and K. Kitao, *Nucl. Data Sheets* **97**, 765 (2002).
- [49] B. Singh, *Nucl. Data Sheets* **93**, 33 (2001).
- [50] B. Singh and Hu. Zhiqiang, *Nucl. Data Sheets* **98**, 335 (2003).
- [51] B. Singh, *Nucl. Data Sheets* **109**, 297 (2008).
- [52] D. De Frenne, *Nucl. Data Sheets* **110**, 1745 (2009).
- [53] J. Blachot, *Nucl. Data Sheets* **108**, 2035 (2007).
- [54] D. De Frenne and A. Negret, *Nucl. Data Sheets* **109**, 943 (2008).
- [55] J. Blachot, *Nucl. Data Sheets* **91**, 135 (2000).
- [56] Yu. Khazov, A. A. Rodionov, S. Sakharov and B. Singh, *Nucl. Data Sheets* **104**, 497 (2005).
- [57] A. A. Sonzogni, *Nucl. Data Sheets* **103**, 1 (2004).
- [58] B. Singh, *Nucl. Data Sheets* **75**, 199 (2003).
- [59] S.-c. Wu and H. Niu, *Nucl. Data Sheets* **100**, 483 (2003).
- [60] B. Singh and J. C. Roediger, *Nucl. Data Sheets* **111**, 2081 (2010).
- [61] C. M. Baglin, *Nucl. Data Sheets* **111**, 275 (2010).
- [62] C. M. Baglin, *Nucl. Data Sheets* **99**, 1 (2003).
- [63] B. Singh, *Nucl. Data Sheets* **95**, 387 (2002).
- [64] B. Singh, *Nucl. Data Sheets* **99**, 275 (2003).
- [65] B. Singh, *Nucl. Data Sheets* **113**, 1871 (2006).
- [66] H. Xiaolong, *Nucl. Data Sheets* **108**, 1093 (2007).
- [67] L. K. Peker and J. K. Tuli, *Nucl. Data Sheets* **82**, 187 (1997).
- [68] N. Nica, *Nucl. Data Sheets* **117**, 1 (2014).
- [69] S. K. Basu and A. A. Sonzogni, *Nucl. Data Sheets* **114**, 435 (2013).
- [70] M. J. Martin, *Nucl. Data Sheets* **114**, 1497 (2013).
- [71] C. W. Reich, *Nucl. Data Sheets* **110**, 2257 (2009).
- [72] C. W. Reich, *Nucl. Data Sheets* **113**, 2537 (1995).
- [73] A. El Batoul, M. Oulne, and I. Tagdamte, *J. Phys. G: Nucl. Part. Phys.* **48**, 085106 (2021).
- [74] A. A. Raduta and P. Baganu, *J. Phys. G: Nucl. Part. Phys.* **40**, 025108 (2013).
- [75] S. Ait El Korchi, M. Chabab, A. El Batoul, and M. Oulne, *Europhys. Lett.* **132**, 52001 (2021).
- [76] A. E. L. Dieperink and R. Bijker, *Phys. Lett. B* **116**, 77 (1982).